Fracture Toughness Testing at Cryogenic Temperatures

STP 496

ASTM

AMERICAN SOCIETY FOR TESTING AND MATERIALS

FRACTURE TOUGHNESS TESTING AT CRYOGENIC TEMPERATURES

A symposium
presented at the
Seventy-third Annual Meeting
AMERICAN SOCIETY FOR
TESTING AND MATERIALS
Toronto, Ontario, Canada, 21–26 June 1970

ASTM SPECIAL TECHNICAL PUBLICATION 496

List price $5.00

04-496000-30

AMERICAN SOCIETY FOR TESTING AND MATERIALS
1916 Race Street, Philadelphia, Pa. 19103

Library of Congress Catalog Card Number: 70-163001

NOTE

The Society is not responsible, as a body,
for the statements and opinions
advanced in this publication.

Printed in Baltimore, Md.
August 1971

Foreword

Committee E-24 on Fracture Testing of Metals sponsored the Symposium on Fracture Toughness Testing at Cryogenic Temperatures at the Seventy-third Annual Meeting of the American Society for Testing and Materials, held in Toronto, Ontario, Canada, 21–26 June 1970. The two-session meeting, given on 24 June, was chairmaned by J. G. Kaufman of the Alcoa Research Laboratories, who was assisted by J. F. Boysen of the Boeing Company.

Related ASTM Publications

Fracture Toughness Testing and Its Applications, STP 381 (1965), $19.50

Plane Strain Crack Toughness Testing of High Strength Metallic Materials, STP 410 (1967), $5.50

Review of Developments in Plane Strain Fracture Toughness Testing, STP 463 (1970), $18.50

Contents

Introduction

This special technical publication consists of four papers presented at the Symposium on Fracture Toughness Testing at Cryogenic Temperatures at the 1970 Annual Meeting of the American Society for Testing and Materials, held in Toronto, Canada. The session was conceived by the Low Temperature Panel of the ASTM-ASME Joint Committee on Effect of Temperature on the Properties of Metals and cosponsored and supported by ASTM Committee E-24 on Fracture Testing of Metals and the Aerospace Panel of the Joint Committee.

The symposium was organized to provide a current picture of the state of the art in fracture toughness testing at cryogenic temperatures. Of principal interest was the application of the foundation of fracture toughness testing, based upon modified linear elastic fracture mechanics and built by ASTM Committee E-24, to the field of ultralow temperatures. The four papers in this volume are representative of the situation today. The Vishnevsky-Steigerwald and Nelson-Kaufman papers describe direct applications of the ASTM plane-strain fracture toughness test method (E 399 - 70) to cryogenic evaluations, although the temperature control procedures used in that program (carried out several years ago) are not recommended today. The paper by L. R. Hall presents comparative fracture toughness data for several different specimen designs, including those covered by the ASTM method and surface flawed specimens, at various temperatures. The fourth, by Orange et al, moves more strongly into the complex area of surface flaws now being attacked by ASTM Committee E-24 and presents an analytical treatment of cryogenic data.

The Vishnevsky-Steigerwald paper merits special attention, as it is the result of a program developed by the Low Temperature Panel and sponsored by the Metal Properties Council with the specific intent of developing cryogenic fracture toughness data suitable for consideration for handbook use. It is the official publication of the final report from that program. All of the detailed data, on file in the Metal Properties Council Office in the Engineering Center in New York City, are available for further study as fracture test methods evolve. The results of this program will also be of special interest to the novice in fracture toughness testing, cryogenic or otherwise. They provide ample evidence of the pitfalls and practical problems that may be encountered in obtaining valid K_{Ic} values.

Three other presentations that do not appear in this volume were made at the symposium:

1. Fracture Behavior of Three Cryogenic Materials (Aluminum Alloys 2021-T81 and 7007-T6 and a Low Silicon Content 301 Stainless steel); by F. R. Schwartzberg, R. D. Keys, and T. F. Keifer; Martin-Marietta Co., Denver, Colo.
2. Extension, Penetration, and Arrest of Cracks in 2014-T6 Aluminum Alloy Welds; by D. E. Schaub, R. A. Rawe, and R. S. Wrath; McDonnell-Douglas Corp., Santa Monica, Calif.
3. Stress Wave Emissions During Subcritical Crack Growth in Beryllium at −320 F; by A. T. Green and C. E. Hartbower; Aerojet-General Co., Sacramento, Calif.

These papers are not presented in this volume principally because they are not compatible with ASTM style and concepts. They do, however, contain valuable information in certain specialized fields. Interested persons are referred to the authors for copies of the original manuscripts.

It is appropriate here to express, on behalf of the Low Temperature Panel, our gratitude to the Aerospace Panel of the Joint Committee and ASTM Committee E-24 for their support of this symposium and, especially, to the Metal Properties Council for their funding of the program leading to first report in this volume. Also, special thanks are due J. A. Boysen for his assistance in setting up the program and cochairmaning the symposium.

J. G. Kaufman
Alcoa Research Laboratories
New Kensington, Pa.

C. Vishnevsky[1] *and E. A. Steigerwald*[1]

Plane Strain Fracture Toughness of Some Cryogenic Materials at Room and Subzero Temperatures

REFERENCE: Vishnevsky, C. and Steigerwald, E. A., "**Plane Strain Fracture Toughness of Some Cryogenic Materials at Room and Subzero Temperatures,**" *Fracture Toughness Testing at Cryogenic Temperatures, ASTM STP 496*, American Society for Testing and Materials, 1971, pp. 3–26.

ABSTRACT: An investigation was conducted to measure the plane strain fracture toughness, K_{Ic}, of eight potential cryogenic service alloys at 75, −100, and −321 F. The test materials included 7039-T61 and 2021-T81 aluminum alloys, Ti-6Al-4V STA in both alpha+beta and beta processed conditions, and the following steels: ASTM A553-A, PH 13-8Mo (H 1150-M), HP 9-4-20, and 18Ni (200 grade) maraging.

Results include both fracture toughness and tensile data as a function of test temperature for each alloy, together with overall comparisons in terms of the plane strain crack size factor, $(K_{Ic}/\sigma_{ys})^2$, versus yield strength and yield strength to density ratio.

In cases where valid K_{Ic} data could not be generated, the appropriate aspects of the ASTM Tentative Method of Test for Plane Strain Fracture Toughness of Metallic Materials (E 399 - 70T) are discussed.

KEY WORDS: cryogenics, aluminum alloys, titanium alloys, steels, structural steels, strains, stresses, fractures (materials), toughness, tensile properties, bend properties, notch sensitivity, yield strength, cracking (fracturing), density (mass/volume), design, bend tests, tension tests

The subject of linear elastic fracture mechanics has been widely studied by many investigators for over a decade. A particularly useful outgrowth of this effort has been the development of the plane strain fracture toughness, K_{Ic}, as a measure of crack propagation resistance, principally in high strength materials. This parameter is a useful design tool because it permits a quantitative relationship to be expressed between critical flaw size and applied stress in terms of material properties, K_{Ic}, and yield strength.

[1] Principal engineer and manager, respectively, Materials Research Department, TRW Inc., Equipment Group, Cleveland, Ohio 44117.

In spite of the fact that considerable information has been published on the fracture toughness of various alloys, there is a dearth of reliable K_{Ic} data for many high strength structural alloys. This situation has arisen because many of the available data were obtained using techniques now known to introduce significant inaccuracies.

During the past several years, ASTM Committee E-24 on Fracture Testing of Metals has been developing standard procedures for K_{Ic} testing and a tentative test method, E 399 - 70T, was recently published [1]. In view of the complexity of the subject, some eventual modifications to this procedure are anticipated. However, the basic techniques are now sufficiently well developed to enable the systematic generation of reliable K_{Ic} data for many materials.

The work described here was initiated by the Low Temperature Panel of the ASTM-ASME Joint Committee on the Effect of Temperature on the Properties of Metals primarily to obtain design K_{Ic} data on potential cyrogenic service alloys. Eight alloys representing three widely differing classes of materials were included in the program. The results of these tests, together with some observations and comments related to the current test method, are presented in the following sections.

Materials and Procedure

Eight materials representing steel, aluminum, and titanium alloy were evaluated in this investigation. These are listed in Table 1, which also shows the vendor, the thickness of the as-received stock, and its chemical analysis. With the exception of the HP 9-4-20 and 18Ni (200 grade) maraging steels all alloys were obtained in a fully heat treated condition. The HP 9-4-20 steel was quenched and tempered at TRW, while the maraging steel was received in an annealed condition that necessitated aging after machining of the test specimens. Table 2 gives a summary of the data available on the processing of the test materials.

Tensile and notch bend fracture toughness properties were determined at 75 F in an ordinary air environment, at -100 F in either acetone or ethanol-dry ice baths,[2] and at -321 F by submersion in liquid nitrogen. The specimens were machined with their longitudinal axes perpendicular to the primary working direction, that is, in the WR orientation. For the tension tests, conventional threaded end, unnotched bars having a test section diameter of 0.505 in. and a gage length of 2.0 in. were tested, with a minimum of two tests conducted at each temperature.

Fracture toughness tests were performed to determine the plane strain fracture toughness, K_{Ic}, using procedures developed by ASTM Committee E-24 as ASTM E 399. The toughness specimens were fatigue precracked

[2] Acetone was used for all tension testing, while ethanol was used for the notch bend tests to avoid possible damage to the clip gage used to monitor crack opening displacement.

TABLE 1—*Test materials and chemical composition.*

Alloy	Vendor	Heat No.	Plate Thickness, in.	Composition, wt% (TRW check analyses in parentheses)											
7039-T61 aluminum	Kaiser	140101	2	Si	Fe	Cu	Mn	Mg	Cr	Zn	Ti				
				0.30 max	0.40 max	0.10 max (0.04)	0.10/ 0.40	2.3/ 3.3 (2.50)	0.15/ 0.25	3.5/ 4.5 (3.75)	0.10	(Specified Range)			
2021-T81 aluminum	Alcoa	...	1	Cu	Fe	Si	Mn	Mg	Zn	Zr	V	Ti	Cd	Sn	
				6.08 (6.00)	0.11	0.07	0.25 (0.30)	0.00 (0.05)	0.03	0.13 (0.18)	0.08	0.05	0.14	0.03	
Ti-6Al-4V STA ($\alpha + \beta$ processed)	Timet	K-2564	1⅛	C	Fe	N	H	O	Al	V					
				0.022	0.15	0.010	0.007 (0.003)	0.17 (0.18)	6.1	4.1					
Ti-6Al-4V STA (β processed)	Timet	G-9131	1	C	Fe	N	H	O	Al	V					
				0.024	0.18 (0.13)	0.013	0.005 (0.008)	0.20 (0.16)	6.2 (6.1)	4.2 (4.12)					
ASTM A553-A steel	Armco	48344-P2942	3	C	Mn	Si	Ni	P	S						
				(0.07)	(0.62)	(0.19)	(8.94)	(0.009)	(0.010)						
PH 13-8Mo (H 1150-H) steel	Armco	1W0328	1¾	C	Mn	Si	Cr	Ni	Mo	Al	P	S			
				0.047	0.04	0.02	12.90 (12.85)	8.36 (8.06)	2.16 (2.24)	1.19	0.002	0.002			
18Ni maraging steel (200 grade)	Inco	...	2⅛	C	Mn	Si	Cr	Ni	Mo	Co	Al	Ti	P	S	
				0.005	0.03	0.02	0.10	18.4	3.34	8.5	0.07	0.20	0.005	0.008	
HP 9-4-20 steel	Republic	3910513	1½	C	Mn	Si	Cr	Ni	Mo	Co	Cu	V	P	S	
				0.17 (0.21)	0.20	0.01	0.74	9.12 (8.90)	0.92	4.35 (4.24)	0.14	0.07	0.009	0.007	

notched bars tested in three-point bending. The relative dimensions of a notch bend fracture toughness specimen are illustrated in Fig. 1. The specimen thickness, B, corresponded to the thickness dimension of the rolled plate after removal of scale or surface imperfections. The other specimen dimension, W, the width or height, and S, the span length between supports, were integral multiples of B.

Virtually all notch bend bars were prepared with a straight-through starter notch configuration. An initial slot having a width of approximately 0.070 to 0.100 in. was introduced with a thin grinding wheel. The base of this slot was extended an additional 0.050 to 0.070 in. by electric discharge machining. The width of the extension was 0.010 to 0.015 in. For all nonferrous materials, integrally machined, beam-type clip gage attachment knife edges were used, while for the steels single-edge razor blades or cutting blades were spot welded to the specimen surface slot opening. Care was taken to ensure that the distance between spot welds on either side of the slot did not exceed the limits permitted for screw holes of removable knife edges [*1*].

The base of the EDM slot extension was sharpened by fatiguing in cantilever bending, using a Sonntag SF 1-U machine for all 1-in.-thick specimens and an SF-4 machine for the larger test specimens. Although

TABLE 2—*Processing history of test materials.*

Alloy	Summary of Processing or Heat Treatment[a]
7039-T61 aluminum	Solution at 850 F (~2½ h), water quench; age at room temperature (~8 h); age at 320 F (18 h).
2021-T81 aluminum	Solution at 985 F (2 h), oil quench; preage at 300 F (1 h); stretch 1.5% maximum; age at 325 F (24 h).
Ti-6Al-4V ($\alpha + \beta$ processed and β processed)	Solution at 1725 to 1750 F (1 h), water quench; age at 1000 F (4 h).
ASTM A553-A steel	Initially cross rolled at longitudinal to transverse reduction ratio of 7.11 to 1. Heat treated as follows: austenitize at 1475 F (4½ h), oil quench; temper at 1100 F (5¾ h), oil quench.
PH 13-8Mo steel (H 1150-M)	Condition austenite at 1400 F (2 h), air cool; 1150 F (4 h), air cool.
18Ni maraging steel (200 grade)	Anneal at 1650 F (2 h), air cool; anneal at 1450 F (2 h), air cool; age at 900 F (2 h).
HP 9-4-20 steel	Normalize at 1650 F (1½ h), air cool; austenitize at 1500 F (1½ h), water quench; temper at 1025 F (6 h).

[a] Actual processing information was available only for 2021-T81 aluminum and the A553-A, maraging, and HP 9-4-20 steels; for other materials the conventional specified treatments are shown.

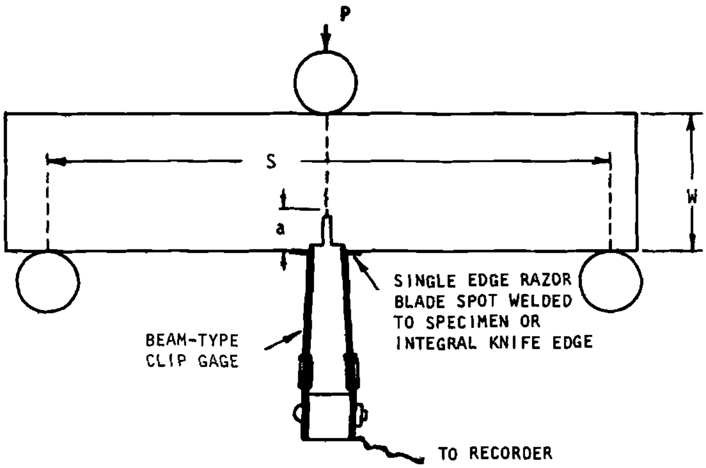

$$K_Q = \frac{P_Q S}{B W^{3/2}} \left[2.9\left(\frac{a}{W}\right)^{1/2} - 4.6\left(\frac{a}{W}\right)^{3/2} + 21.8\left(\frac{a}{W}\right)^{5/2} - 37.6\left(\frac{a}{W}\right)^{7/2} + 38.7\left(\frac{a}{W}\right)^{9/2} \right]$$

P_Q = Load obtained from test record, lbs.
B = Specimen thickness, in.
W = Specimen width, = 2B
S = Span length, = 4W
a = Crack length (machined notch plus fatigue crack), in.
K_Q = Conditional plane strain fracture toughness, psi$\sqrt{\text{in}}$
K_Q = K_{Ic} (plane strain fracture toughness), if all criteria for valid test are satisfied.

FIG. 1—*Schematic representation of notch bend fracture toughness test setup and equation used to calculate fracture toughness.*

cantilever loading can cause crack inclination and is thus less preferable than symmetrical loading, in none of the specimens did the angular difference between the crack surface and starter notch plane of symmetry exceed the maximum permissible value of 10 deg [*1*].

Care was taken to ensure that the amount of fatigue crack extension and the maximum stress intensity level during the terminal stages of precracking, $K_{f(max)}$, were in accord with the tentative test method. Prior to precracking the bulk of the material, a number of preliminary K_{Ic} tests were performed at −321 F to facilitate estimates of the highest stress intensity levels that could be applied in precracking at room temperature. The actual stress intensity values were calculated to an estimated accuracy of better than ±5 percent using published [2] K calibration curves for cantilever bending at crack length to width ratios, a/W, up to 0.50. Extrapolations of these curves to $a/W = 0.55$ were used for two of the test materials. In addition to departing from the currently recommended procedure with respect to the method of loading during precracking, the ratio of minimum to maximum load was not maintained at a maximum value of 0.10 but, instead, was in the range of 0.19 to 0.25. The latter difference is also not expected to have seriously affected the K_{Ic} values.

Fracture toughness tests were performed in a three-point bending fixture in which the support rolls, initially held against stops by low tension leaf springs, were permitted to roll apart on hardened plane surfaces. This arrangement essentially eliminates frictional effects. A beam-type clip gage was attached to the previously described knife edges at the specimen edge. A minimum of three tests were performed at each test temperature. During the actual test a chart record of applied load, P, versus clip gage output was generated. From this record a load value, P_Q, was obtained and used to calculate a conditional plane strain fracture toughness value, K_Q. Examples of three different types of test records are shown in Fig. 2. In each case a line OA is drawn along the initial straight line portion of the test record. A second line OP_5 is drawn at a slope 5 percent less than that of OA and P_Q is defined as the maximum load in the test record up to or including the intercept point P_5.

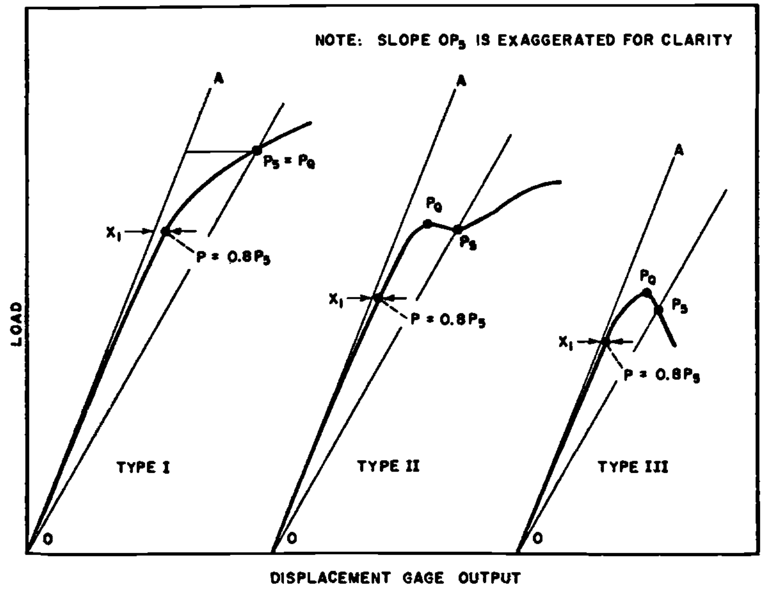

FIG. 2—*Principal types of load-displacement records* [1].

A K_Q value based on P_Q is rejected as a valid K_{Ic} if the deviation of the test record from line OA at a load of $0.8P_5$ is greater than one fourth of the deviation from linearity of the test record at P_5. In addition to this requirement, various other criteria must be satisfied. The two most important of these are that both the specimen thickness, B, and crack length, a, must not be less than $2.5(K_Q/\sigma_{ys})^2$, where σ_{ys} is the 0.2 percent offset yield strength. Details of other criteria regarding specimen preparation, precracking conditions, the straightness of the fatigue crack front, a/W ratio, and test procedure may be obtained from the published tentative test method.

The following sections discuss the results of the tension and K_{Ic} tests on the various alloys.

Results and Discussion

The results of individual notch bend fracture toughness tests for all alloys are summarized in Table 3. Some of the data were not valid K_{Ic} and are only denoted as K_Q. In such instances the specific criterion for valid K_{Ic} testing that was not satisfied is identified.

For purposes of presentation the materials were classified into the following categories:

1. Aluminum alloys, 7039-T61 and 2021-T81.
2. Titanium alloy, Ti-6Al-4V STA, in both $\alpha + \beta$ and β processed conditions.
3. High strength steels, HP 9-4-20 and 18Ni (200 grade) maraging.
4. Medium strength steels, ASTM A553-A and PH 13-Mo (H 1150-M).

Aluminum Alloys

The tensile and fracture toughness properties of the 7039-T61 and 2021-T81 alloys are shown in Figs. 3 and 4, respectively. The tensile data consist of the tensile strength, yield strength, and reduction of area, while the fracture toughness test results are presented only as K_{Ic}. A number of invalid K_Q values for the 2021-T81 alloy, identified in Table 3, were not plotted in Fig. 4. When the degree of scatter between individual test results was slight, the data in both figures were presented as averages, with a notation for the number of tests included.

Both aluminum alloys exhibited an increase in K_{Ic} with decreasing test temperature. For the 7039-T61 alloy, this beneficial effect of low temperature on K_{Ic} was small and possibly not significant, while for 2021-T81 the K_{Ic} at -321 F was about 40 percent greater than the room temperature value. At 75 and -100 F the lower strength 7039-T61 alloy provided appreciably higher toughness, while at -321 F the K_{Ic} of the 2021-T81 alloy was greater, 31.8 versus 30.5 ksi$\sqrt{\text{in.}}$

TABLE 3—*Fracture toughness test results.*

Material	Test No.	Temperature, deg F	0.2% Yield Strength, ksi	K_Q,[a] ksi$\sqrt{\text{in.}}$	K_{Ic},[b] ksi$\sqrt{\text{in.}}$
7039-T61 aluminum.....	AK-1	75	48.8	29.0	29.0
	2			29.2	29.2
	3			30.0	30.0
				avg	29.4
	AK-4	−100	52.5	29.6	29.6
	6			29.6	29.6
	7			29.9	29.9
				avg	29.7
	AK-5	−321	58.4	29.8	29.8
	9			31.3	31.3
	10			30.5	30.5
	11			30.4	30.4
				avg	30.5
2021-T81 aluminum.....	BK-2	75	61.3	22.8	22.8
	3			23.1	23.1
	4			22.5	22.5
				avg	22.8
	BK-1	−100	65.4	27.0	27.0
	5			26.0	26.0
	6			26.4	... (1)
	7			26.8	... (1)
	8			26.4	26.4
				avg	26.5
	BK-10	−321	73.2	32.6	32.6
	11			32.2	... (4)
	13			30.9	30.9
	14			32.1	... (4)
				avg	31.8
Ti-6Al-4V STA ($\alpha + \beta$ processed)......	CK-1	75	161.2	35.4	... (1, 4)
	2			38.4	... (4)
	12			33.5	... (4)
	CK-3	−100	187.0	39.7	... (4)
	4			37.4	... (4)
	11			41.2	... (4)
	CK-6	−321	238.0	32.9	... (4)
	7			32.3	... (4)
	9			32.5	... (4)
	10			32.0	... (4)
Ti-6Al-4V STA (β processed)...........	DK-1	75	150.3	39.1	39.1
	9			45.9	45.9
	11			49.6	49.6
				avg	44.9

TABLE 3—*Continued.*

Material	Test No.	Temperature, deg F	0.2% Yield Strength, ksi	K_Q,[a] ksi $\sqrt{in.}$	K_{Ic},[b] ksi $\sqrt{in.}$
	DK-3	−100	178.1	44.9	44.9
	4			45.7	45.7
	10			49.0	49.0
				avg	46.5
	DK-5	−321	227.3	37.7	37.7
	6			34.0	34.0
	7			35.2	35.2
	8			36.5	36.5
				avg	35.9
18Ni maraging steel (200 grade)............	GK-3	75	205.7	168.3	168.3
	4			172.4	172.4
	5			168.7	168.7
				avg	169.8
	GK-6	−100	229.5	167.1	167.1
	7			158.1	158.1
	8			166.1	166.1
				avg	163.8
	GK-9	−321	271.4	85.7	85.7
	10			77.0	77.0
	11			73.5	73.5
				avg	78.7
HP 9-4-20 steel.........	HK-1	75	183.6	126.3	... (1)
	8			125.3	... (1)
	10			120.6	... (1)
	HK-2	−100	197.8	134.9	134.9
	4			138.2	... (1)
	11			129.1	129.1
				avg	132.0
	HK-6	−321	240.5	50.6	50.6
	7			50.8	50.8
	9			46.0	46.0
				avg	49.1
ASTM A553-A steel.....	EK-2	75	92.3	95.0	... (1, 3, 4)
	3			101.5	... (1, 2, 4)
	6			100.5	... (1, 2, 4)
	11			101.4	... (1, 2, 4)
	EK-5	−100	96.6	99.8	... (1, 3, 4)
	9			98.5	... (1, 4)
	10			96.3	... (1, 3, 4)
	EK-4	−321	124.5	114.1	... (1, 4)
	7			100.8	... (1, 4)
	12			106.5	... (1, 4)

TABLE 3—*Continued.*

Material	Test No.	Temperature, deg F	0.2% Yield Strength, ksi	K_Q,[a] ksi $\sqrt{\text{in.}}$	K_{Ic},[b] ksi $\sqrt{\text{in.}}$
PH 13-8Mo (H 1150-M) steel	FK-2	75	84.5	55.1	... (1)
	5			46.1	... (1)
	6			65.3	... (1)
	FK-7	−100	100.5	...[c]	... (1)
	9			...[c]	... (1)
	10			...[c]	... (1)
	FK-8	−321	144.4	68.3	... (1)
	11			80.8	... (1)
	14			76.3	... (1)
	15			68.6	... (1)

Applicable Criteria for Valid K_{Ic}	Section in ASTM Test Method E 399 - 70T
1. fails deviation from linearity criterion (excessive test record curvature)	8.1.2
2. insufficient crack length or thickness or both	8.1.5
3. crack length to width ratio, a/W, outside the limits 0.45 to 0.55	6.2.1
4. nonuniform fatigue crack front	7.2.3

[a] Conditional plane strain fracture toughness.

[b] Valid plane strain fracture toughness; numbers in parentheses identify criteria for valid K_{Ic} that were not satisfied.

[c] Because of extreme curvature in the test record an initial straight line portion was not defined and P_Q could not be established.

Titanium Alloy, Ti-6Al-4V

The solution treated and aged Ti-6Al-4V alloy was evaluated in two prior processing conditions, which resulted in appreciably different microstructures. Figure 5 compares the structure of the alpha + beta processed material, containing primary alpha grains of a semicontinuous nature in a beta matrix, with that of the essentially beta processed material, whose structure consisted of alpha platelets in a Widmanstätten array in a beta matrix. The latter structure is probably the consequence of rolling near or at the beta transus.

The results of tension and fracture toughness tests of Ti-6Al-4V are summarized in Figs. 6 and 7. The acicular structure exhibited slightly lower tensile and yield strengths at all temperatues and lower ductility at −100 and −321 F. Valid K_{Ic} values were obtained at each test temperature. These were nearly equal at 75 and −100 F but dropped considerably at −321 F.

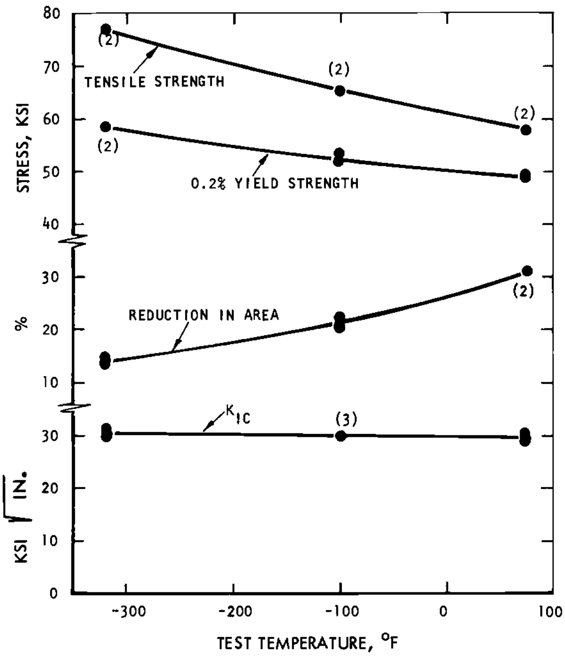

FIG. 3—*Smooth tensile properties and fracture toughness of 7039-T61 aluminum alloy. Parentheses denote the numbers of overlapping data points.*

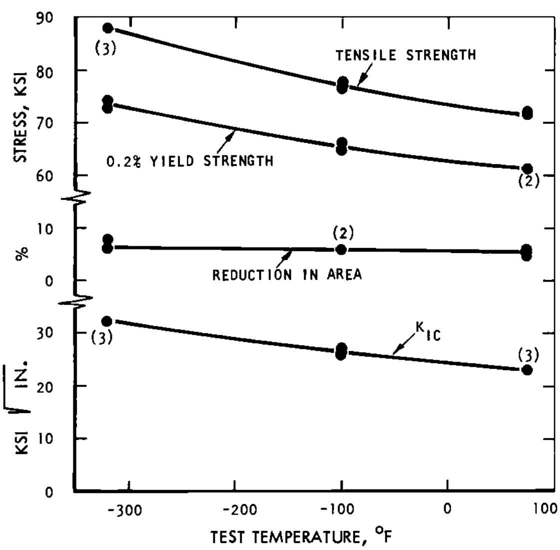

FIG. 4—*Smooth tensile properties and fracture toughness of 2021-T81 aluminum alloy. Parentheses denote the numbers of overlapping data points.*

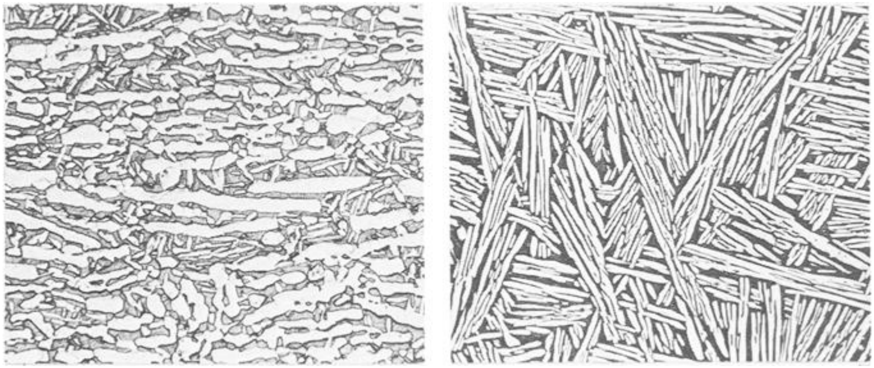

FIG. 5—*Microstructure of Ti-6Al-4V alloy test material (×340): left, $\alpha + \beta$ processed, lot C; right, β processed, lot D.*

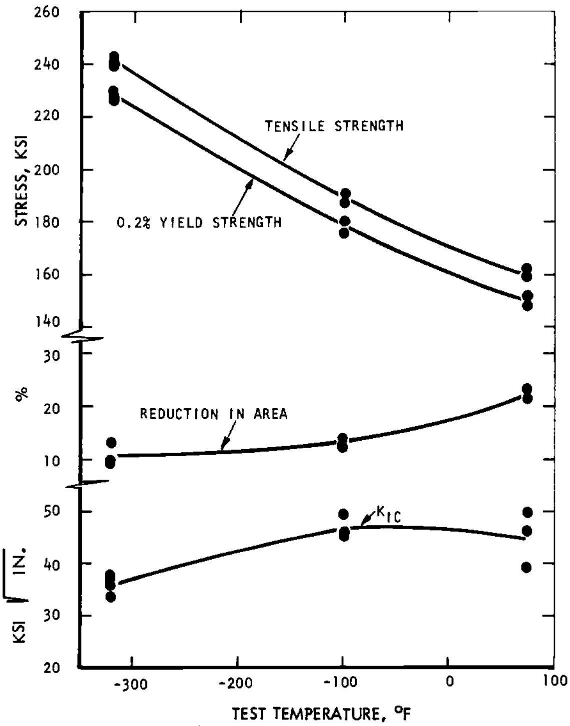

FIG. 6—*Smooth tensile properties and fracture toughness of beta processed, solution treated, and aged Ti-6Al-4V.*

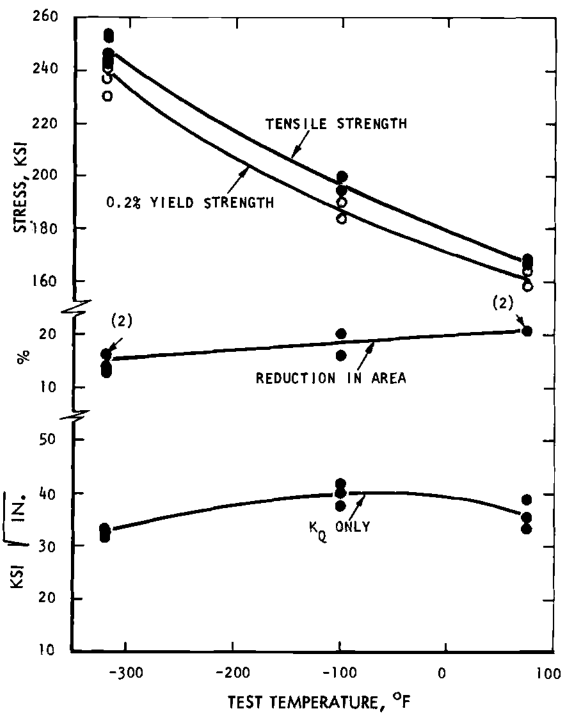

FIG. 7—*Smooth tensile properties and fracture toughness of alpha + beta processed, solution treated, and aged Ti-6Al-4V. Parentheses denote the number of overlapping data points.*

However, for the $\alpha + \beta$ processed material no valid K_{Ic} data were generated, because sufficiently uniform fatigue crack fronts could not be obtained. For all specimens the crack length measurements at the specimen surface were less than 90 percent of the average crack length based on three interior readings (center and quarter points). A deviation of this magnitude in crack straightness is unacceptable in a valid K_{Ic} test. Typical examples of crack fronts for the $\alpha + \beta$ and β processed materials are compared in Fig. 8. These large differences in crack growth behavior are not attributed to precracking technique but probably reflect variations in material properties. Similar anomalous crack growth behavior for Ti-6Al-4V having different microstructures has been observed by Hickey and DeSisto.[3]

No method currently exists for correcting for the effects of pronounced crack front curvature. However, if it is assumed that the K_Q results for the $\alpha + \beta$ processed structure closely approximate K_{Ic}, then the relative

[3] Private communication with C. F. Hickey, Jr., and T. S. DeSisto, Army Materials and Mechanics Research Center, Watertown, Mass., November 1970.

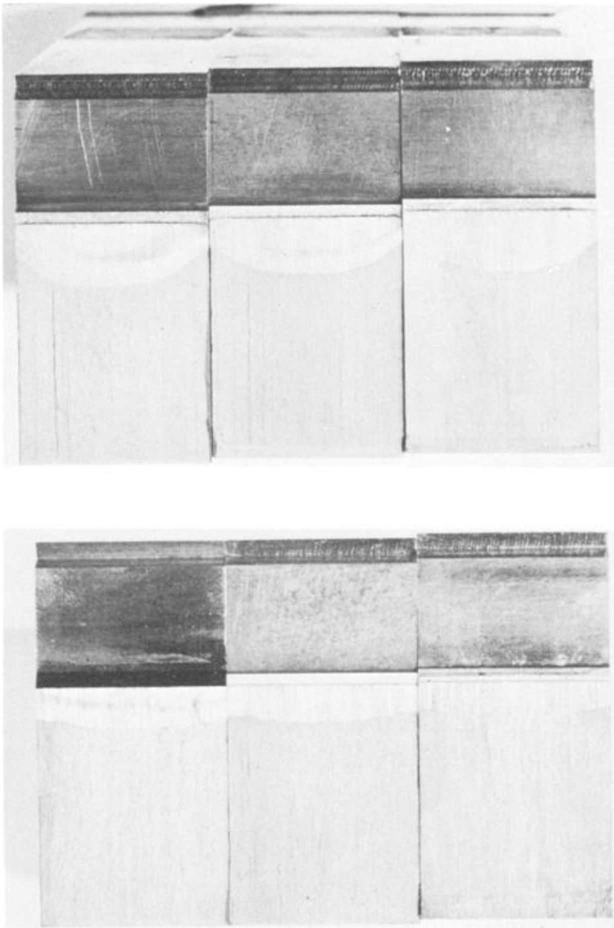

FIG. 8—*Typical fatigue crack front shapes in Ti-6Al-4V. Top, $\alpha + \beta$ processed, lot C; bottom, β processed, lot D. Left 75 F, center −100 F, and right −321 F.*

toughness of the two conditions is consistent both with the higher strength $\alpha + \beta$ processed material and the results of other investigators showing a toughness superiority after β processing [*3*]. However, it should be emphasized that, because the materials represent different heats, the effects of processing may be confounded by other variables, notably, differences in the level of interstitial impurities, so that the two conditions are not strictly comparable.

High Strength Steels

The results of tension and fracture toughness tests on the HP 9-4-20 and 18Ni (200 grade) maraging steels are summarized in Figs. 9 and 10, respectively. For the HP 9-4-20 steel valid K_{Ic} data were not obtained at 75 F and one of three tests at -100 F was rejected. In each case the load-displacement curves exhibited excessive curvature so the deviation from linearity criterion was not satisfied. However, the required minimum thickness and crack length in these tests as calculated from $2.5(K_Q/\sigma_{ys})^2$ were less than the actual dimensions. This suggests that K_Q underestimated K_{Ic}, particularly at 75 F where the average K_Q was less than K_{Ic} at -100 F.

In the case of the maraging steel, valid K_{Ic} data were obtained with all test specimens. In terms of both strength and toughness it provided a better combination of properties than did HP 9-4-20, since at all temperatures the yield strength was 10 to 15 percent higher with no sacrifice in toughness. Although for both alloys K_{Ic} values at -321 F were considerably lower than at -100 F, the maraging steel exhibited a fracture toughness at -321 F that was approximately 50 percent higher than that for HP 9-4-20.

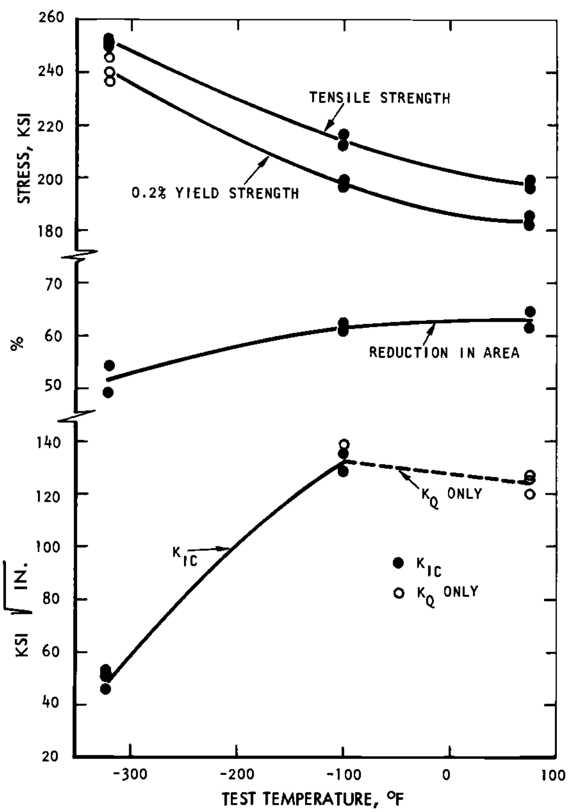

FIG. 9—*Smooth tensile properties and fracture toughness of HP-9-4-20 steel.*

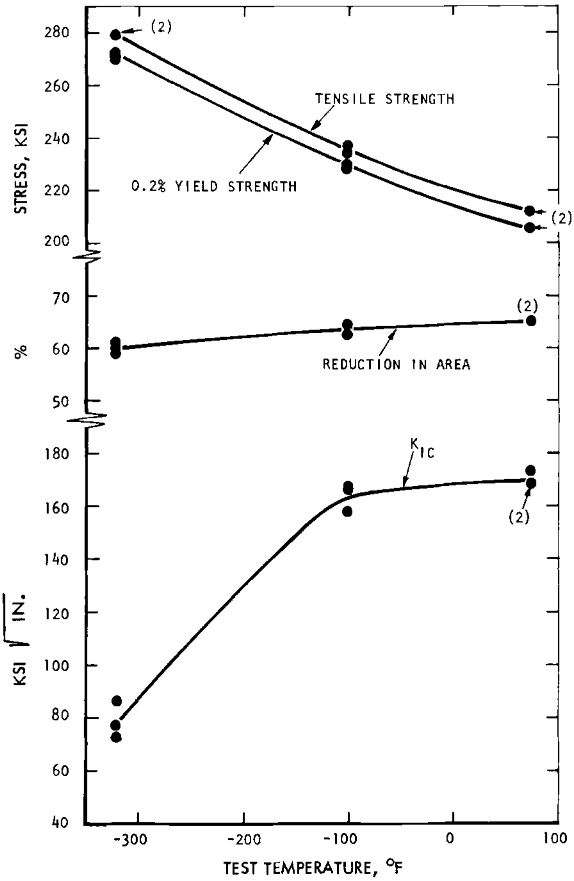

FIG. 10—*Smooth tensile properties and fracture toughness of 18Ni (200 grade) maraging steel. Parentheses denote the numbers of overlapping data points.*

Medium Strength Steels

Figures 11 and 12 show the effect of temperature on strength, ductility, and fracture toughness of the ASTM A553-A and PH 13-8Mo (H 1150-M) steels. The toughness values are in all cases K_Q, since no valid K_{Ic} data were obtained.

For the PH 13-8Mo steel the primary reason for rejecting the data was failure to satisfy the deviation from linearity criterion. Curvature of the test records was particularly pronounced at 75 and −100 F, and the intercept loads, P_Q, were generally one third or less of the maximum load in the test. This situation was more severe at −100 F, and an initial slope *OA* (see Fig. 2) could not be determined. Accordingly, P_Q was not measured for these tests. At −321 F curvature of the test record was appreciably less, because the yield strength was higher and the intrinsic K_{Ic} level was probably lower than at 75 or -100 F. The effect of this improved test record linearity was to increase P_Q to a higher value than was obtained at 75 F, thus causing an apparent rise in toughness with decreasing test temperature. Figure 13 shows the appearance of the test record from one of the -321 F tests. A distinct popin was observed at a load above P_Q.

Both at 75 and -321 F the criteria that the crack length and thickness must not be less than $2.5(K_Q/\sigma_{ys})^2$ were satisfied. As in the case of the HP 9-4-20 steel, these K_Q values probably underestimated K_{Ic}, with the -321 F data being closer to K_{Ic} because of less test record curvature.

For the ASTM A553-A steel excess plasticity, as revealed by the test record, also occurred in all tests. Furthermore, every specimen exhibited a nonuniform crack front of the type observed for $\alpha + \beta$ processed Ti-6Al-4V. In the A553-A steel the crack curvature does not appear to be the result of precracking conditions, and it was not alleviated by varying the starter notch configuration. Figure 14*a* shows a typical crack front of an

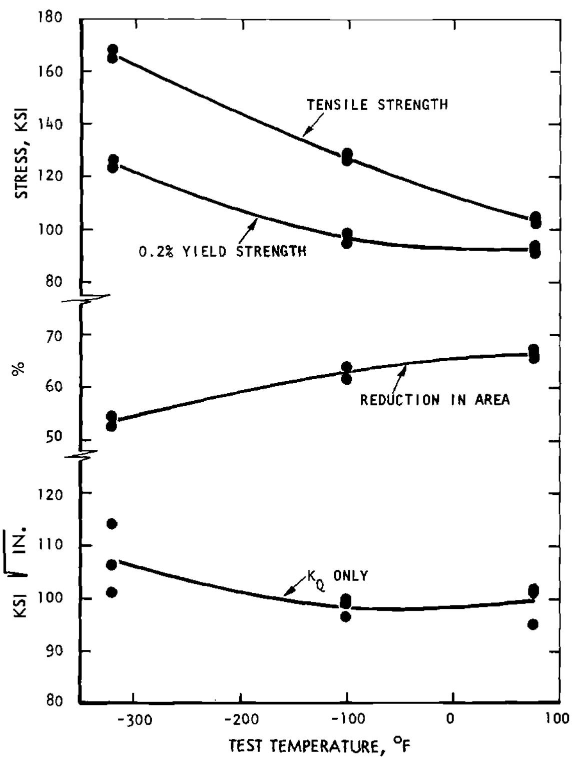

FIG. 11—*Smooth tensile properties and fracture toughness of ASTM A553-A steel. Parentheses denote the numbers of overlapping data points.*

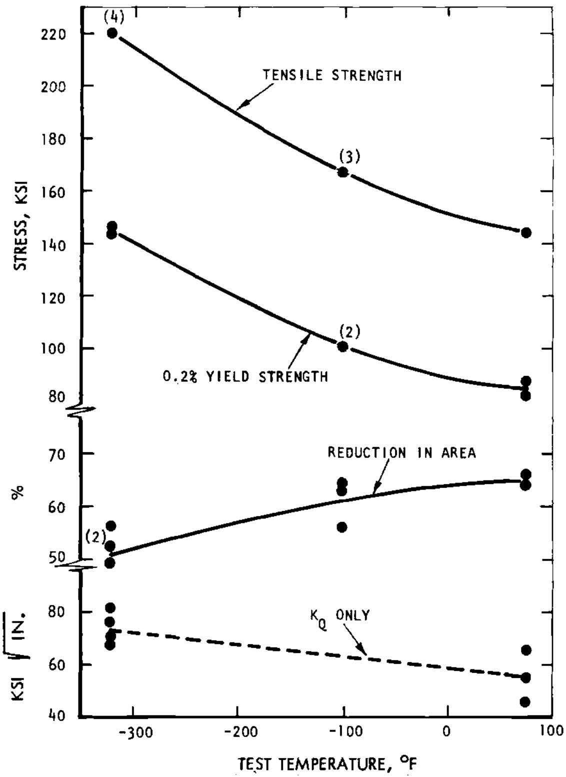

FIG. 12—*Smooth tensile properties and fracture toughness for PH 13-8Mo (H 1150-M) steel. Parentheses denote the numbers of overlapping data points.*

A553-A steel specimen prepared with a straight-through starter notch, while Fig. 14*b* illustrates the crack front obtained with a chevron starter notch. In both cases the crack was severely advanced at the specimen interior. A third specimen, Fig. 14*c*, was prepared with sharp ⅛-in.-deep side grooves to accelerate crack growth at the specimen surfaces. These grooves were machined off prior to testing. In spite of some acceleration of crack growth at the surfaces, the crack front was still unacceptable. Thus it appears that this condition was caused by structural variations across the thickness which influenced the rate of fatigue crack growth.

Comparison of Various Alloys

The fracture toughness properties of all eight materials are compared in Fig. 15 in terms of the plane strain crack size factor, $(K_{Ic}/\sigma_{ys})^2$, versus yield strength. The crack size factor was selected in place of K_{Ic}, because

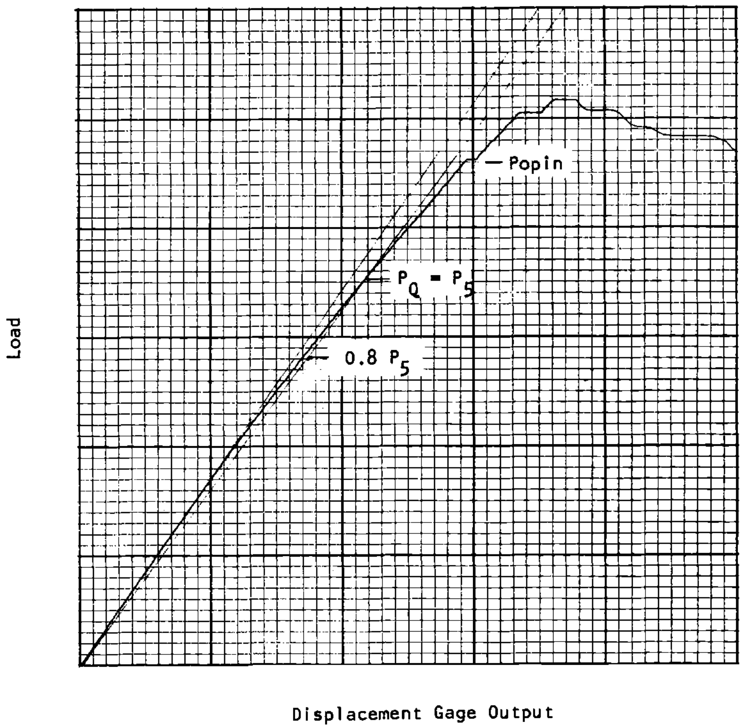

FIG. 13—*Load-displacement record for a PH 13-8Mo specimen (FK-15) tested at −321 F showing 5% secant intercept load,* P_Q, *considerably below the popin load. This test record failed to satisfy the linearity criterion at 0.8*P_5.

it provides a measure of toughness that accounts in a single parameter for the interactions of K_{Ic} and strength on crack size tolerance.[4] This figure includes data for all three test temperatures; an increase in yield strength for any alloy is associated with a reduction in test temperature. K_Q results for $\alpha + \beta$ processed Ti-6Al-4V and the PH 13-8Mo and A553-A steels are also included in the figure.

The relative toughness of the aluminum alloys is different in this representation than in comparisons based on K_{Ic}. At all temperatures the crack size factor of the 7039-T61 alloy is appreciably higher than that of 2021-T81, although it should be noted that the latter exhibits higher strength. Also, 2021-T81 is the only material for which the crack size factor increased with decreasing temperature. Of the medium strength steels, A553-A had

[4] The crack size factor is not related to critical crack size at a stress equal to the yield strength but only under small-scale yielding, that is, at applied stresses appreciably below the yield strength [4].

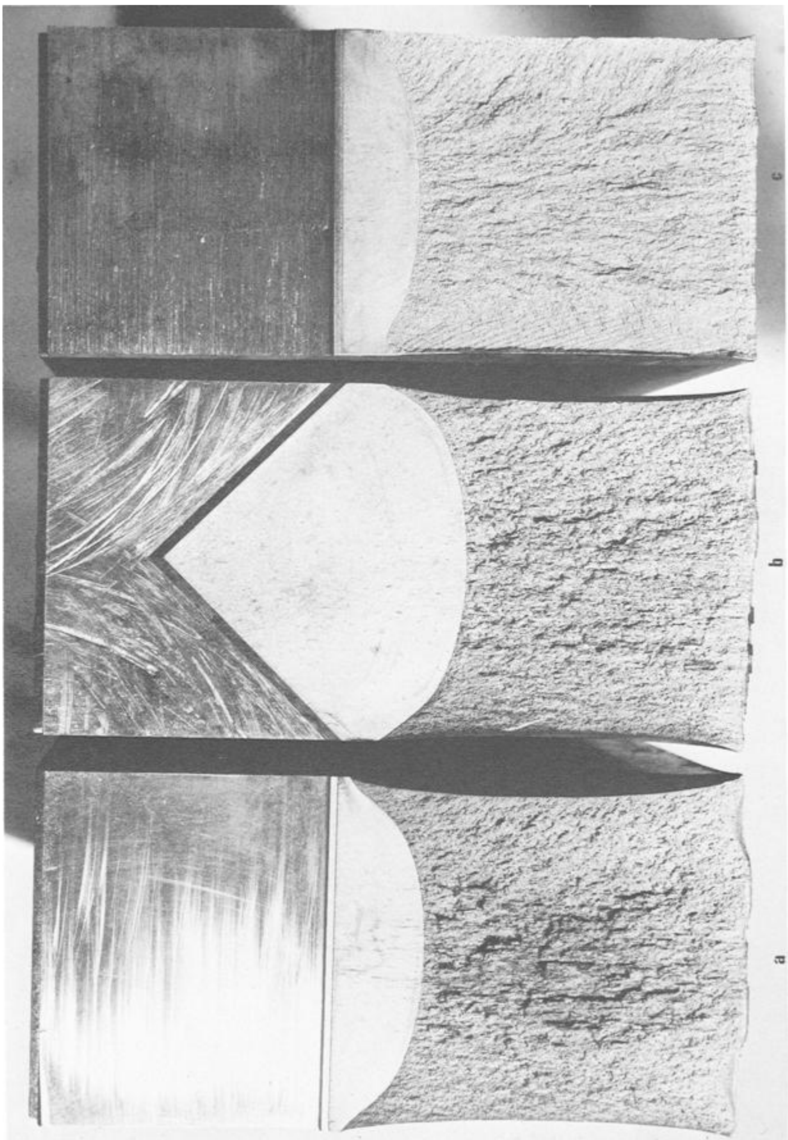

FIG. 14—*Fatigue crack fronts obtained in ASTM A533-A steel specimens with different starter notch configurations: (a) straight-through notch, (b) chevron notch, (c) straight-through notch plus side grooves (machined off prior to testing).*

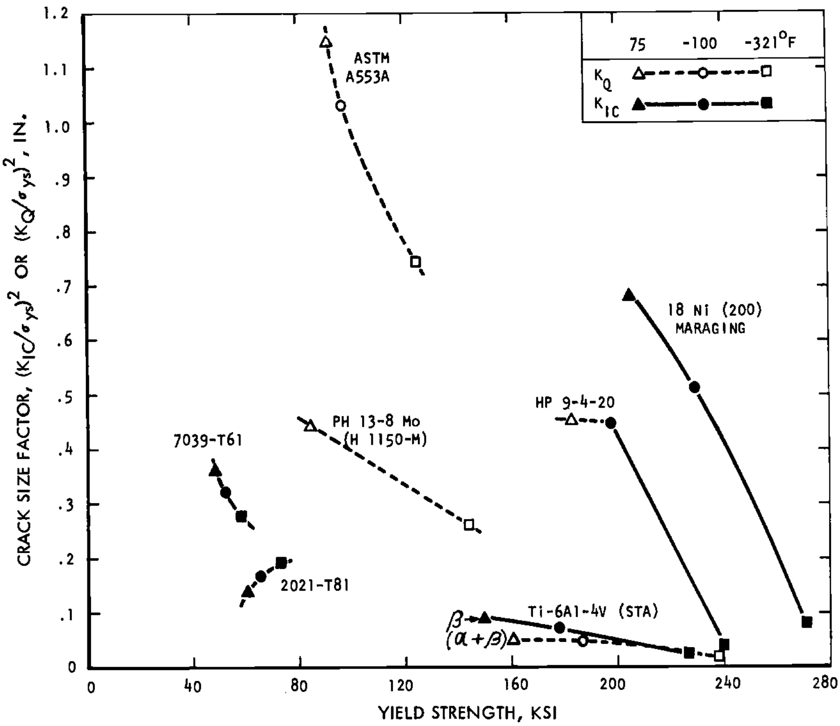

FIG. 15—*Variation of crack size factor with yield strength for all materials tested.*

a considerably higher crack size factor than did PH 13-8Mo and the highest crack size factor of any material tested. Because valid K_{Ic} data were not obtained for either of these steels, such comparisons are only approximate. In the case of the high strength steels, the maraging steel provided a distinct advantage over HP 9-4-20 in terms of both strength and toughness. At −321 F the crack size factor of the maraging steel was nearly twice that of HP 9-4-20.

In certain applications strength to weight considerations are important, and it is then convenient to compare materials on the basis of crack size factor versus yield strength to density ratio. Figure 16 shows that, if compensation is made for differences in density, different relative behavior is evident. The Ti-6Al-4V alloy exhibited the highest strength to density ratio but a low crack size factor. However, of the other materials, the maraging steel remained distinctly superior at 75 F and −100 F. Figure 17 shows only the −321 F points from the previous plot. This graph more clearly indicates the range of material selection which is available for cryogenic service from a strength to weight consideration.

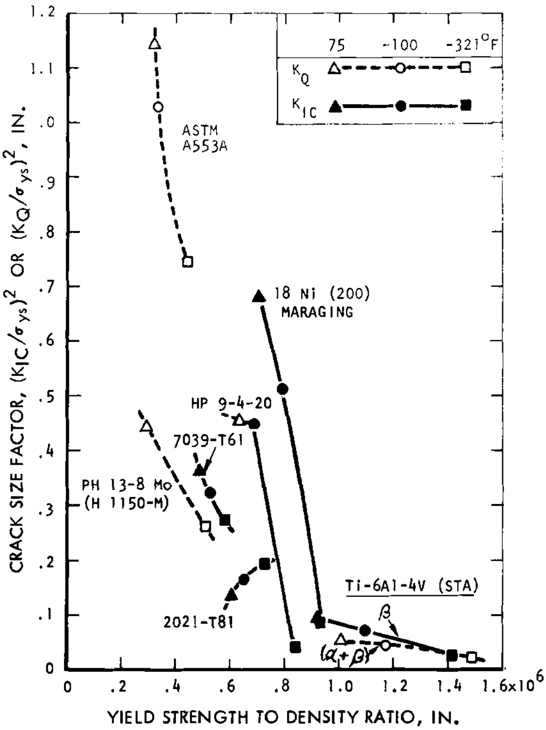

FIG. 16—*Variation of crack size factor with yield strength to density ratio for all materials tested.*

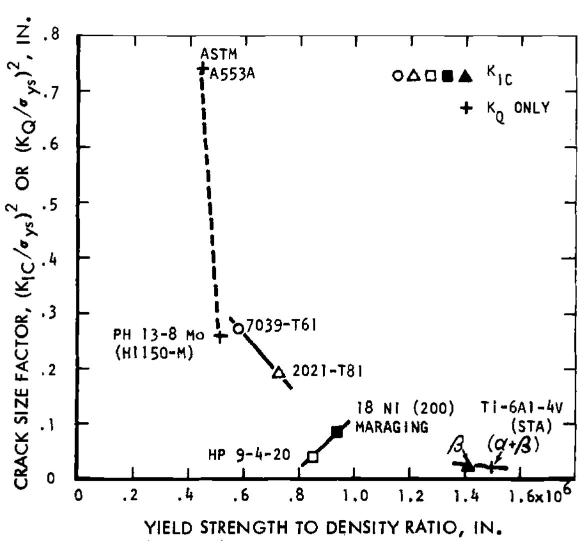

FIG. 17—*Variation of crack size factor with yield strength to density ratio at −321 F.*

General Considerations

In addition to providing data on the fracture toughness of various alloys, the results of this study suggest some comments regarding the present method for K_{Ic} testing, E 399 - 70T.

As discussed previously, the difficulties encountered in obtaining sufficiently straight crack fronts for two materials, $\alpha + \beta$ processed Ti-6Al-4V STA and the A553-A steel, were probably caused by material characteristics and not precracking conditions. The consistency of crack growth behavior for all specimens of a particular alloy and the consistent differences between alloys, as well as the insensitivity of crack growth to starter notch configuration, add support to this contention. The limits on crack front curvature which now exist in the test method might be relaxed if analytical or experimental data on the effect of crack shape were available.

Another major cause for invalid K_{Ic} results was excess plasticity in the test record. This nonlinearity was indicative of slow crack growth or plastic zone extension because of insufficient specimen size or both. A feature of these results was that, in most cases where the linearity criterion was not satisfied, the additional requirements that crack length and thickness must not be less than $2.5(K_Q/\sigma_{ys})^2$ indicated adequate size. In fact, for 25 tests that failed the linearity test, only three failed the size requirement.

Jones and Brown [5] have shown that within the scope of the present test method K_Q values for subsize specimens can either overestimate or underestimate K_{Ic}. For all tests in this study, in which crack length and thickness were nearly equal, an undersized specimen would tend to underestimate K_{Ic}. Usefulness of the $2.5(K_Q/\sigma_{ys})^2$ test is implicitly based on the assumption that K_{Ic} is known or K_Q will tend to overestimate it. But obviously, if K_Q greatly underestimates K_{Ic}, this criterion may give the false indication that specimen size is adequate, and the sole burden for revealing insufficient thickness and crack length is placed on an unambiguous interpretation of the test record.

Summary and Conclusions

An investigation was conducted to measure the plane strain fracture toughness, K_{Ic}, of eight potential cryogenic service alloys at 75, -100, and -321 F. The test materials included 7039-T61 and 2021-T81 aluminum alloys, Ti-6Al-4V STA in both $\alpha + \beta$ processed conditions, and the following steels: ASTM A553-A, PH 13-8Mo (H 1150-M), HP 9-4-20, and 18Ni (200 grade) maraging. Valid K_{Ic} data were obtained for five materials, while for the remainder (Ti-6Al-4V ($\alpha + \beta$), PH 13-8Mo, and ASTM A553-A) one or both of the following conditions, test record nonlinearity and insufficiently straight fatigue crack fronts, were primarily responsible for invalidating the results.

Of the aluminum alloys, 2021-T81 provided the higher strength at all temperatures and a slight toughness advantage in terms of K_{Ic} over 7039-

T61 at −321 F. However, on the basis of the crack size factor, $(K_{Ic}/\sigma_{ys})^2$, the latter was more crack tolerant at all temperatues. For Ti-6Al-4V the lower sterngth and higher toughness of the Widmanstätten structure in comparison with a more equiaxed $\alpha + \beta$ microstructure is consistent with information in the literature on a toughness superiority for beta processing, although the absence of valid data for the $\alpha + \beta$ condition (due only to insufficient crack front straightness) obviously precludes a definite comparison.

The 18Ni (200 grade) maraging steel provided the highest yield strength and excellent toughness. In comparison with a similar strength steel, HP 9-4-20, it exhibited the better overall combination of strength and toughness, particularly at −321 F. For two medium strength steels, ASTM A553-A and PH 13-8Mo (H 1150-M), valid K_{Ic} data could not be generated. In addition to difficulties in obtaining uniform fatigue crack fronts in the A553-A steel (which alone is sufficient to invalidate the data), both materials exhibited considerable test record curvature because of insufficient specimen size. Nevertheless, the toughness of these materials appears to be high, with the A553-A steel having the highest crack size factor, $(K_Q/\sigma_{ys})^2$, of any alloy in this study.

In terms of increasing K_{Ic} alone, the materials can be rated in the following general order: aluminum alloys, Ti-6Al-4V, and steels. However, because of appreciable differences in both strength and density a comparison in terms of plane strain crack size factor, $(K_{Ic}/\sigma_{ys})^2$, versus yield strength to density ratio indicated certain regimes of usefulness for each alloy.

Acknowledgments

This work was performed for the Low Temperature Panel of the ASTM-ASME Joint Committee on Effect of Temperature on the Properties of Metals under Metal Properties Council Contract J69-1. The test materials were provided through the courtesy of the following companies: Aluminum Corporation of America, Armco Steel Corporation, International Nickel Company, Kaiser Aluminum and Chemical Corporation, Republic Steel Corporation, and Titanium Metals Corporation of America.

References

[1] Tentative Method of Test for Plane Strain Fracture Toughness of Metallic Materials (E 399 - 70T), *Annual Book of ASTM Standards*, Vol. 31, American Society for Testing and Materials, 1970, p. 911.

[2] Fisher, D. M. and Repko, A. J., *Materials Research and Standards*, MTRSA, Vol. 9, No. 5, May 1969, p. 28.

[3] Heitman, G. H., Coyne, J. E., and Galipeau, R. P., *Metals Engineering Quarterly*, MENQA, Vol. 8, No. 3, Aug. 1968, p. 15.

[4] Brown, W. F., Jr., and Srawley, J. E. in *Review of Developments in Plane Strain Fracture Toughness Testing, ASTM STP 463*, American Society for Testing and Materials, 1970, p. 216.

[5] Jones, M. H. and Brown, W. F., Jr., in *Review of Developments in Plane Strain Fracture Toughness Testing, ASTM STP 463*, American Society for Testing and Materials, 1970, p. 63.

F. G. Nelson[1] *and J. G. Kaufman*[1]

Plane Strain Fracture Toughness of Aluminum Alloys at Room and Subzero Temperatures

REFERENCE: Nelson, F. G. and Kaufman, J. G., "**Plane Strain Fracture Toughness of Aluminum Alloys at Room and Subzero Temperatures,**" *Fracture Toughness Testing at Cryogenic Temperatures, ASTM STP 496*, American Society for Testing and Materials, 1971, pp. 27–39.

ABSTRACT: Plane strain fracture toughness tests have been made at room temperature, −112, and −320 F on plates of six aluminum alloys and tempers: 2014-T651, 2024-T851, 6061-T651, 7075-T651, 7075-T7351, and 7079-T651. The data indicate that the plane strain fracture toughness, K_{Ic}, of each of the alloys at the subzero temperatures is as high as or higher than that at room temperature. At −320 F apparently valid values of K_{Ic} ranged from 4 (7075-T7351) to 23 percent (2014-T651 and 7075-T651) higher than at room temperature. An even larger difference was indicated for 6061-T651 (about 40 percent higher), but the specimens tested at −320 F were not thick enough to satisfy the requirements of ASTM Test E 399 - 70 T. For the alloys of most interest for cryogenic applications, 2014-T651 and 6061-T651, the critical crack sizes at cryogenic temperatures are indicated to be as large as or larger than those at room temperature when evaluated at either a fixed operating stress or a constant percentage of the yield strength.

KEY WORDS: cracking (fracturing), fatigue (materials), fracture tests, toughness, strains, plastic properties, tensile properties, cryogenics, temperature, yield strength, aluminum alloys

Certain aluminum alloys are recognized as well suited for cryogenic applications, principally because they exhibit higher strength as temperature decreases but no abrupt transition in fracture mode associated with large decreases in fracture energy over a narrow temperature range [*1, 2*]. Even for the high strength aluminum alloys which do exhibit a change in fracture appearance from oblique to flat as reductions in temperature lessen the size of the plastic zone with respect to the thickness of the structure, no abrupt change in fracture resistance, nor more specifically

[1] Research engineer and chief, respectively, Mechanical Testing Division, Alcoa Research Laboratories, New Kensington, Pa. 15068.

TABLE 1—*Average long transverse tensile properties at room temperature, −112, and −320 F of some aluminum alloy plate used for fracture toughness tests.*

Alloy and Temper	Temperature, deg F	Tensile Strength, ksi	Yield Strength,[a] ksi	Elongation in 2 in., %
2014-T651	75	72.0	65.8	9.2
	specified min[b]	67.0	59.0	6
	−320	86.0[c]	75.0[c]	...
2024-T851	75	70.8	64.4	7.2
	specified min[d]	64.0	56.0	5
	−112	76.0	69.2	6.8
	−320	87.7	79.0	7.5
6061-T651	75	51.0	43.4	12.0
	specified min[b]	42.0	35.0	8
	−112	50.1	45.5	12.0
	−320	57.9	47.2	16.8
7075-T651	75	86.1	77.7	10.8
	specified min[b]	77.0	67.0	6
	−112	91.4	82.8	9.2
	−320	104.0	92.0	5.8
7075-T7351	75	68.2[e]	56.8[e]	12.0
	specified min	69.0	57.0	6
	−112	73.8	59.1	11.0
	−320	87.4	66.0	10.8
7079-T651	75	82.5	72.8	11.2
	specified min[b]	73.0	64.0	8
	−112	89.9	81.2	10.2
	−320	100.6	90.6	4.5

[a] Offset equals 0.2 percent.
[b] "Aluminum Standards and Data," The Aluminum Association, 1970–71 edition; ASTM B 209.
[c] Extrapolated from well established typicals.
[d] General Dynamics specification FM 1010.
[e] Fails to meet current minimum values for 7075-T7351 plate.

fracture toughness, has been observed [*3*]. However, only a few data are available [*4*, *5*] on the plane strain fracture toughness, K_{Ic}, as determined by current procedures [*6*], of aluminum alloys at subzero temperatures.

As a preliminary to more extended studies of fracture toughness at low temperatures, including −452 F, Alcoa Research Laboratories has evaluated the fracture toughness of several high strength aluminum alloys including 2014-T651, 2024-T851, 6061-T651, 7075-T651 and T7351, and 7079-T651, with plane strain fracture toughness tests at room temperature, −112, and −320 F.

It is beyond the scope of this paper to describe the development of fracture mechanics concepts and test methods or the application of these data in material selection or design. For this information reference is made to the published reports of ASTM Committee E-24 on Fracture Testing of Metals [*7–12*] and to the three ASTM special technical publications on the subject [13–15]. It will be useful to note, nevertheless, that K_{Ic}, the principal index of toughness used in this paper, is the plane strain fracture toughness as defined in ASTM Test for Plane Strain Fracture Toughness of Metallic Materials (E 399 - 70T); that is, it is the "critical" value of the plane strain stress intensity factor defining the stress field intensity near the tip of an ideal crack in an elastic medium when the crack is opened under tensile loading. Thus, it is considered to be an index of the resistance of the material to unstable crack growth under elastic conditions. The value of K_{Ic} is proportional to the applied load and the square root of the crack length at the critical conditions defined by the test method.

Material

The 2014-T651, 2024-T851, 6061-T651, 7075-T651, 7075-T7351, and 7079-T651 stress relieved aluminum alloy plate used in this investigation was 1 to 1½ in. thick and was fabricated by the normal procedures in use at the time of its production. The tensile properties of most of these specimens, as given in Table 1, are typical of the respective alloy and temper and exceed the respective requirements of applicable federal, military, ASTM, and Aluminum Association specifications. The tensile strength and yield strength of the lot of 7075-T7351 plate fall several hundred psi below the current minimum values; however, this lot of plate was fabricated and tested several years ago and met all the requirements of applicable specifications at that time. The trends in data indicated for this lot are believed to be representative of those for current commercial plate.

Procedure

Plane strain fracture toughness tests were made of plate, nominally 1, 1⅜, or 1½ in. thick, with fatigue cracked, three-point bend fracture toughness specimens of the geometry shown in Fig. 1. The tests were con-

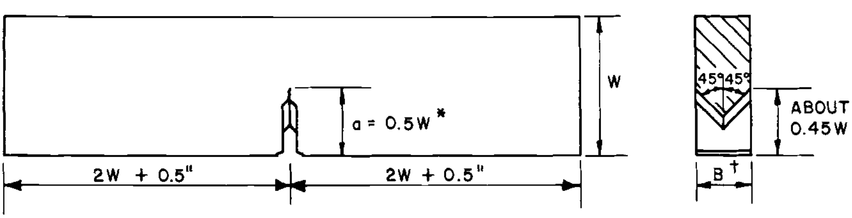

THICKNESS, B, IN.	WIDTH, W, IN.	LENGTH, IN.	CRACK LENGTH, a,* IN.
1	2	9	1
1-3/8	3	13	1-3/8
1-1/2	3	13	1-1/2

FIG. 1—*Fatigue cracked three-point bend fracture toughness specimen.*

ducted in accordance with the procedures in the draft of the then proposed ASTM Method of Test for Plane Strain Fracture Toughness of Metallic Materials current over the period from 1967 to early 1969. These procedures differ in several respects from the current practice of the method as noted below; however, the modifications are not considered to grossly affect the numerical values of the test results. The notch bend specimens were fatigue cracked at stress intensities equal to 10 $\pm$ 2 ksi$\sqrt{\text{in.}}$; they were precracked by fully reversed cantilever bending, using a stress intensity calibration procedure developed by NASA Lewis Research Center and believed to be accurate to within $\pm$5 percent. Present ASTM practices require the use of symmetrical loading during fatigue cracking.

At room temperature, the static loading of the fatigue cracked specimens was carried out at rates and by procedures which are described in the ASTM method, utilizing a bend device which permits both rotation and translation of the specimen ends (Fig. 2). Crack opening displacements were measured by clip gages mounted on the integrally machined knife edges of the specimens, and load-displacement curves were plotted on an X-Y plotter. Load values for calculating plane strain stress intensity factors were determined at a 5 percent secant offset. Values of K_Q (candidate values of K_{Ic}) were calculated and checked by all the criteria of the cur-

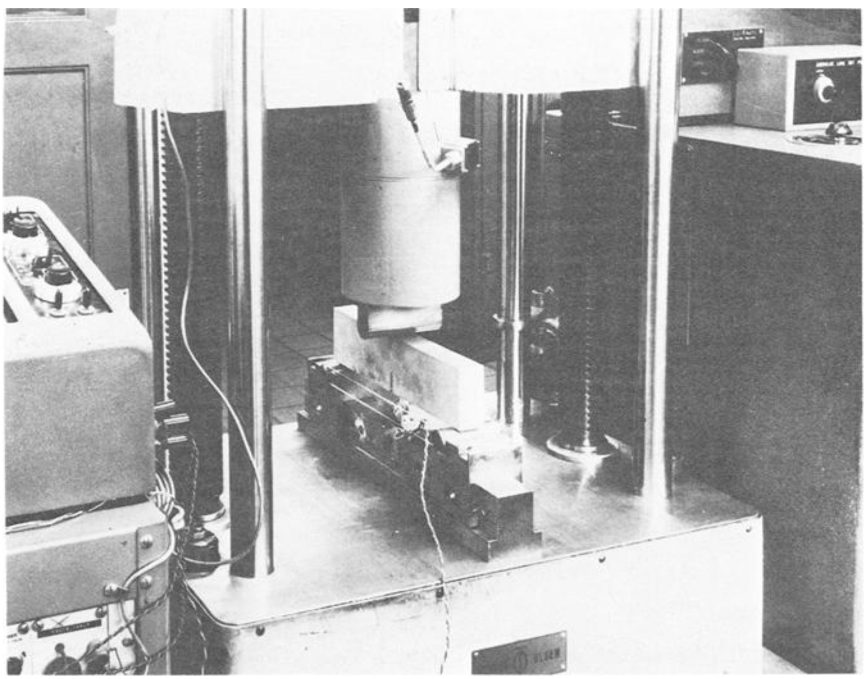

FIG. 2—*Bend device for plane strain fracture toughness tests at room temperature.*

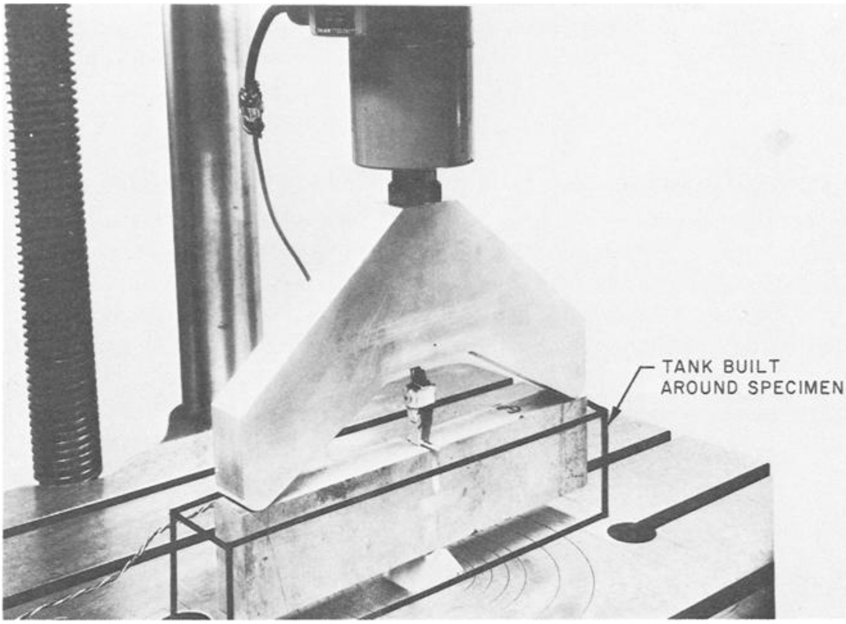

FIG. 3—*Bend device for plane strain fracture toughness tests at subzero temperature.*

rent ASTM test to determine whether or not they could be considered as valid K_{Ic} values. The equation for calculating K_{Ic} was as follows:

$$K_{Ic} = P_Q S/BW^{1/2}[2.9(a/W)^{1/2} - 4.6(a/W)^{3/2} + 21.8(a/W)^{5/2} - 37.6(a/W)^{7/2} + 38.7(a/W)^{9/2}]$$

where

P_Q = load at 5 percent secant offset, lb,
B = thickness of specimen, in.,
S = specimen length, in.,
W = depth of specimen, in., and
a = crack length after fatigue cracking, in.

The tests at −112 and −320 F followed the same procedures as those at room temperature, except that a different type of bend device was used (Fig. 3) in which the specimen was inverted so that the notch was in an upward position and the clip gage projected above the specimen.[2] The assembly was held in a tank containing the appropriate cooling medium. For the tests at −112 F, the temperature was obtained by allowing the liquid nitrogen (LN_2) to boil at a controlled rate. For the tests at −320 F,

[2] Comparison tests showed that the inverted bend device resulted in K_{Ic} values differing by 5 percent from those from the standard ASTM device (Fig. 2), the difference due presumably to friction at the load points.

the specimen was immersed in LN_2 to a level near the top of the specimen and well above the notch in the specimen. Temperature was monitored with thermocouples mounted on the sides of the specimen near the end of the fatigue crack and was within ±5 F of the desired value.

It is recognized that the calibration of the clip gage may have changed slightly as a result of the proximity of the nitrogen vapor or liquid. However, it was stable; and the shift, if any, would not have affected the values of K_{Ic}, since a change in gage signal of 5 percent secant offset is used in calculating K_{Ic} values.

All of the specimens were taken from the plate in the WL orientation, that is, the plane of the crack was normal to the width or long transverse direction, and the crack propagated along the length or longitudinal direction.

Discussion of Results

The results of the individual notch bend tests at room temperature, −112, and −320 F are shown in Table 2 for each of the alloys and tempers. Note that only a few tests were made of certain alloys at the low temperatures (and in one case, none at −112 F) because of the small quantity of material available. The average values of K_{Ic} are plotted in Figs. 4 through 6. Representative fracture surfaces from tests at room temperature and −320 F are shown in Fig. 7.

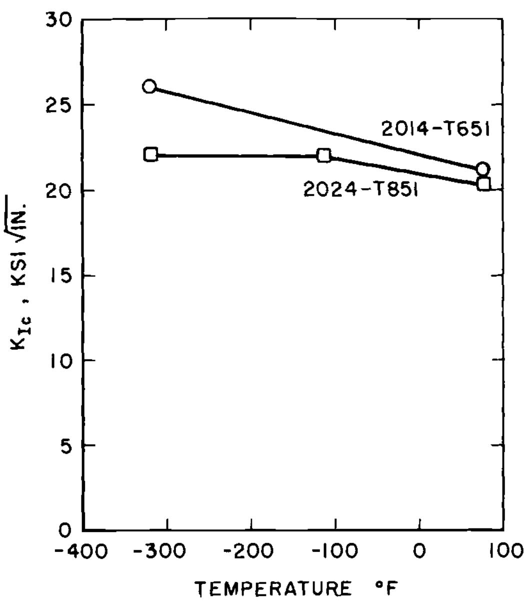

FIG. 4—K_{Ic} *versus temperature for 1 and 1⅜-in. 2XXX series alloy plate (WL orientation).*

TABLE 2—*Results of plane strain fracture toughness tests of aluminum alloy plate with notch bend specimens.*

Alloy and Temper	Nominal Thickness, B, in.	Nominal Width, W, in.	Room Temperature				
			Actual Thickness, in.	Crack Length,[a] in.	K_Q,[b] ksi$\sqrt{\text{in.}}$	$2.5\left(\frac{K_Q}{\sigma_{ys}}\right)^2$,[c] in.	Meaningful K_{Ic}[d]
2014-T651	1	2	1.016	0.989	20.9	0.26	Yes
			1.016	0.985	20.9	0.26	Yes
			1.016	0.998	22.6	0.29	Yes
			1.016	0.970	21.0	0.25	Yes
			1.016	1.001	20.7	0.24	Yes
			avg		21.2	0.25	Yes
2024-T851	1⅜	3	1.388	1.507	20.2	0.24	Yes
			1.385	1.508	20.5	0.25	Yes
			1.387	1.512	20.1	0.24	Yes
			avg		20.3	0.24	Yes
6061-T651	1½	3	1.479	1.443	25.4	0.86	Yes
			1.479	1.508	27.6	1.01	Yes
			...	...	...	...	...
			avg		26.5	0.94	Yes
7075-T651	1⅜	3	1.385	1.575	21.3	0.36	Yes
			1.386	1.519	22.6	0.38	Yes
			1.385	1.566	21.1	0.36	Yes
			1.385	1.584	19.5	0.33	Yes
			1.385	1.676	19.3	0.34	Yes
			1.387	1.484	19.7	0.33	Yes
			1.387	1.469	20.8	0.35	Yes
			1.387	1.484	20.0	0.33	Yes
			avg		20.5	0.35	Yes
7075-T7351	1⅜	3	1.381	1.557	28.9	0.65	Yes
			1.389	1.498	27.6	0.59	Yes
			1.385	1.538[a]	28.2	0.62	Yes
			avg		28.2	0.62	Yes
7079-T651	1⅜	3	1.385	1.677	23.6	0.26	Yes
			1.380	1.617	22.3	0.24	Yes
			1.380	1.628	24.3	0.28	Yes
			avg		23.4	0.26	Yes

[a] Including at least 0.050 in. of fatigue crack introduced by reversed cantilever beam loading at stress intensities = 10 ± 2 ksi$\sqrt{\text{in.}}$

[b] Candidate value of K_{Ic}, calculated per Ref *6*.

[c] Indicative of minimum specimen thickness and crack length for valid tests and proportional to initial crack length at the yield strength.

[d] Indicated as meaningful when ASTM criteria on specimen thickness and crack length are met; not designated valid since the fatigue cracking procedures and, at the subzero temperature, the load point fixity were not in accordance with 1970 version of ASTM method (see text).

TABLE 2—*Continued.*

Alloy and Temper	Nominal Thickness, B, in.	Nominal Width, W, in.	Room Temperature				
			Actual Thickness, in.	Crack Length,[a] in.	K_Q,[b] ksi$\sqrt{\text{in.}}$	$2.5\left(\frac{K_Q}{\sigma_{ys}}\right)^2$,[c] in.	Meaningful K_{Ic}[d]
2014-T651	1	2	...	...	...	...	...
			...	...	...	...	...
			...	...	...	...	...
			...	...	...	...	...
			...	...	...	...	...
2024-T851	1⅜	3	1.39	1.52	21.3	0.24	Yes
			1.39	1.57	22.7	0.27	Yes
			...	...	...	...	...
			avg		22.0	0.26	Yes
6061-T651	1½	3	1.48	1.51	31.9	1.23	Yes
			1.48	1.50	28.2	0.96	Yes
			1.48	1.45	30.3	1.11	Yes
			avg		30.1	1.10	
7075-T651	1⅜	3	1.39	1.52	22.6	0.19	Yes
			...	...	...	...	...
			...	...	...	...	...
			...	...	...	...	...
			...	...	...	...	...
			...	...	...	...	...
			...	...	...	...	...
			...	...	...	...	...
			avg		22.6	0.19	Yes
7075-T7351	1⅜	3	1.387	1.562	28.2	0.37	Yes
			...	...	...	...	...
			...	...	...	...	...
			avg		28.2	0.37	
7079-T651	1⅜	3	1.383	1.652	27.5	0.23	Yes
			1.385	1.695	24.7	0.19	Yes
			...	...	...	...	...
			avg		26.1	0.21	Yes

[a] Including at least 0.050 in. of fatigue crack introduced by reversed cantilever beam loading at stress intensities = 10 ± 2 ksi$\sqrt{\text{in.}}$

[b] Candidate value of K_{Ic}, calculated per Ref *6*.

[c] Indicative of minimum specimen thickness and crack length for valid tests and proportional to initial crack length at the yield strength.

[d] Indicated as meaningful when ASTM criteria on specimen thickness and crack length are met; not designated valid since the fatigue cracking procedures and, at the subzero temperature, the load point fixity were not in accordance with 1970 version of ASTM method (see text).

TABLE 2—*Continued.*

Alloy and Temper	Nominal Thickness, B, in.	Nominal Width, W, in.	Room Temperature				
			Actual Thickness, in.	Crack Length,[a] in.	K_Q,[b] ksi$\sqrt{\text{in.}}$	$2.5\left(\frac{K_Q}{\sigma_{ys}}\right)^2$,[c] in.	Meaningful K_{Ic}[d]
2014-T651	1	2	1.02	1.01	26.1	0.30	Yes
			...	...	...	...	...
			...	...	...	...	...
			...	...	...	...	...
			...	...	...	...	...
			avg		26.1	0.30	Yes
2024-T851	1⅜	3	1.39	1.49	22.1	0.20	Yes
			1.39	1.48	22.2	0.20	Yes
			...	...	...	...	...
			avg		22.2	0.20	Yes
6061-T651	1½	3	1.48	1.48	37.2	1.56	No
			1.48	1.49	38.6	1.67	No
			1.48	1.44	37.9	1.62	No
			avg		37.9	1.62	No
7075-T651	1⅜	3	1.39	1.58	25.1	0.19	Yes
			...	...	...	...	...
			...	...	...	...	...
			...	...	...	...	...
			...	...	...	...	...
			...	...	...	...	...
			...	...	...	...	...
			...	...	...	...	...
			avg		25.1	0.19	Yes
7075-T7351	1⅜	3	1.39	1.48	30.1	0.52	Yes
			1.39	1.53	29.5	0.50	Yes
			1.39	1.52	28.1	0.45	Yes
			avg		29.2	0.49	Yes
7079-T651	1⅜	3	1.38	1.45	25.9	0.20	Yes
			1.38	1.53	28.2	0.24	Yes
			1.38	1.56	25.9	0.20	Yes
			avg		26.7	0.21	Yes

[a] Including at least 0.050 in. of fatigue crack introduced by reversed cantilever beam loading at stress intensities = 10 ± 2 ksi$\sqrt{\text{in.}}$

[b] Candidate value of K_{Ic}, calculated per Ref *6*.

[c] Indicative of minimum specimen thickness and crack length for valid tests and proportional to initial crack length at the yield strength.

[d] Indicated as meaningful when ASTM criteria on specimen thickness and crack length are met; not designated valid since the fatigue cracking procedures and, at the subzero temperature, the load point fixity were not in accordance with 1970 version of ASTM method (see text).

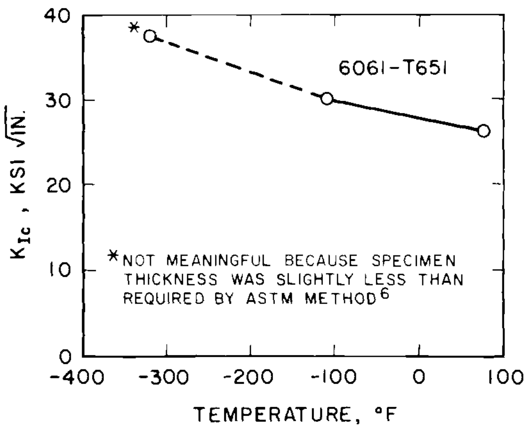

FIG. 5—K_{Ic} *versus temperature for 1½-in. 6061-T651 plate (WL orientation).*

All of the alloys and tempers developed K_{Ic} values at subzero temperatures which were as high as or higher than those at room temperature. For 2024-T851 the K_{Ic} value at −112 F (and at −320 F) was only slightly (8 percent) higher than the room temperature value. For 2014-T651, the value at −320 F (based upon just one test) was 23 percent above the room temperature value.

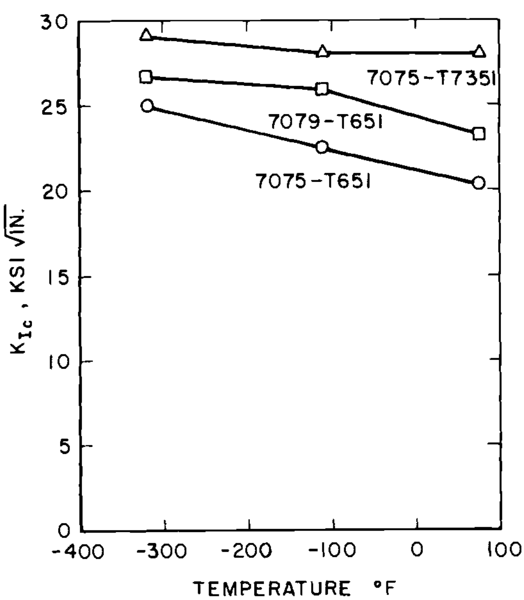

FIG. 6—K_{Ic} *versus temperature for 1⅜-in. 7XXX series alloy plate (WL orientation).*

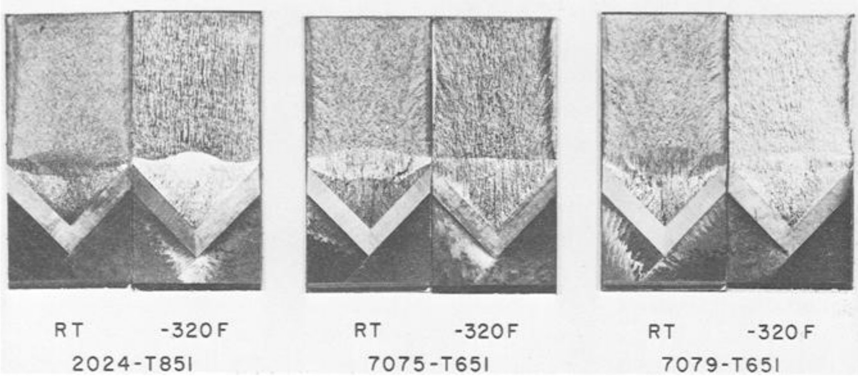

FIG. 7—*Fracture surfaces of fatigue cracked three-point bend specimens of some 1⅜-in.-thick aluminum alloy plate.*

The influence of temperature was greatest for 6061-T6, the values at −112 F averaging 13 percent above the room temperature value and those at −320 F averaging nearly 40 percent higher than the room temperature value. As Table 2 indicates, at −320 F the specimens were not thick enough to meet the current specimen thickness requirements for valid K_{Ic} values, and it is recognized that the values obtained may be either higher or lower than the true K_{Ic} values. Nonetheless, the specimens were only slightly below the required thickness, and it is believed that the values are indicative of the influence of temperature on K_{Ic}. Actually, all the values for 6061-T651 are much lower than might have been expected from other indexes of toughness [7]; hence, they are being studied further.

Within the 7XXX series alloys, the K_{Ic} values for 7075-T651 and 7079-T651 averaged about 11 and 18 percent higher at −112 and −320 F, respectively, than at room temperature. Those for 7075-T7351 were about the same at all three temperatures. Although the values at −320 F for T7351 averaged 4 percent higher than those at room temperature, the individual test results overlapped and the differences may not be significant.

The data indicate that K_{Ic} for all of the alloys at subzero temperatures is at least as high as and generally higher than that at room temperature. The indicated differences are greater for 6061-T651 than for the higher strength 2XXX and 7XXX series of alloys; of the higher strength alloys, the difference was greater for 2014-T651, 7075-T651, and 7079-T651 than for 2024-T851 and 7075-T7351. Of the alloys tested, 2014-T651 and 6061-T651 are of most interest for cryogenic applications, and appreciably higher values of K_{Ic} were indicated for both at cryogenic temperatures.

Conclusions

The trends indicated are generally consistent with other fracture data [2], which indicate that the toughness of most aluminum alloys at subzero temperatures is as high as or higher than that at room temperature. The trend for the 7XXX series may seem inconsistent with the results of tear and notch tension tests, which suggest a modest reduction in toughness with decrease in temperature. However, if the data are viewed in relation to trends in the critical crack length at the yield strength (which is proportional to the square of the K_{Ic}:yield strength ratio), these data do suggest a modest reduction with temperature. For the 2014-T651 and 6061-T651 alloys even this index of toughness indicates higher fracture resistance at cryogenic temperatures than at room temperature.

The implication of these results is that, at a given operating stress, all of the alloys tested can sustain cracks at cryogenic temperatures which are at least as large as and generally larger than those which occur at room temperature. The fracture surfaces support this indication, as there are no obvious changes in the fractographic features of the specimen over the extremes in test temperature. For the principal cryogenic alloys, 2014-T651 and 6061-T651, the critical crack size is indicated to be larger at cryogenic temperatures than at room temperature, even if a constant ratio of stress to yield strength is maintained. Also for these alloys, the critical crack size at the yield strength is greater at cryogenic temperatures than at room temperature, so the structure is as safe as or safer than it is at room temperature in terms of resisting a critical instability at elastic stresses in the event of an accidental overload.

References

[1] Campbell, J. E., *Materials Research and Standards*, MTRSA, Vol. 4, No. 10, Oct. 1964, pp. 540–548.

[2] Kaufman, J. G. and Wanderer, E. T., *Machine Design*, MADEA, Vol. 37, No. 30, 11 Nov. 1965, pp. 199–205.

[3] Begley, J., "Fracture Transition Phenomena," Ph.D. thesis, Lehigh University, 1969.

[4] Pierce, W. S., "Crack Growth in 2014-T6 Aluminum Tensile and Tank Specimens Cyclically Loaded at Cryogenic Temperatures," NASA, Cleveland, April 1968.

[5] Carman, C. M., Forney, J. W., and Katlin, J. M., "Plane Strain Fracture Toughness of 2219-T87 Aluminum Alloy at Room and Cryogenic Temperatures," Pitman-Dunn Research Labs, Frankford Arsenal, Philadelphia, Pa., Aug. 1966.

[6] ASTM Method of Test for Plane Strain Fracture Toughness of Metallic Materials, *Annual Book of ASTM Standards*, Part 31, 1970, pp. 911–927.

[7] Kaufman, J. G. and Holt, Marshall, "Fracture Characteristics of Aluminum Alloys," ARL Technical Paper No. 18, Aluminum Company of America, 1965.

[8] "Fracture Testing of High-Strength Sheet Materials," first report of a special ASTM committee, *ASTM Bulletin*, ASTBA, No. 243, Jan. 1960, p. 29; also, No. 244, Feb. 1960, p. 18.

[9] "The Slow Growth and Rapid Propagation of Cracks", second report of a special ASTM committee, *Materials Research and Standards*, MTRSA, Vol. 1, May 1961, pp. 389–393.

[10] "Fracture Testing of High-Strength Sheet Materials", third report of a special ASTM committee, *Materials Research and Standards*, MTRSA, Vol. 1, Sept. 1961, pp. 877–885.

[11] "Screening Tests for High Strength Alloys Using Sharply Notched Cylindrical Specimens", fourth report of a special ASTM committee, *Materials Research and Standards*, MTRSA, Vol. 2, March 1962, pp. 196–203.

[12] "Progress Is Measuring Fracture Toughness and Using Fracture Mechanics", fifth report of a special ASTM committee, *Materials Research and Standards*, MTRSA, Vol. 4, March 1964, pp. 107–119.

[13] *Fracture Toughness Testing and Its Applications, ASTM STP 381*, American Society for Testing and Materials, 1965.

[14] Brown, W. F., Jr., and Srawley, J. E., *Plane Strain Crack Toughness Testing of High Strength Metallic Materials, ASTM STP 410*, American Society for Testing and Materials, 1967.

[15] *Review of Developments in Plane-Strain Fracture Toughness Testing, ASTM STP 463*, W. F. Brown, Jr., Ed., American Society for Testing and Materials, Sept. 1970.

L. R. Hall[1]

Influence of Specimen Design in Plane Strain Fracture Toughness Testing

REFERENCE: Hall, L. R., "**Influence of Specimen Design in Plane Strain Fracture Toughness Testing,**" *Fracture Toughness Testing at Cryogenic Temperatures, ASTM STP 496*, American Society for Testing and Materials, 1971, pp. 40–60.

ABSTRACT: The influence of specimen design on plane strain fracture toughness (K_{Ic}) was studied by fracturing 2219-T87 aluminum and 5Al-2.5Sn ELI titanium alloy single-edge notched bend (SENB), single-edge notched tension (SENT), compact tension (CT), and surface flawed (SF) specimens at 72 F (295 K) in laboratory air, at −320 F (78 K) in liquid nitrogen, and at −423 F (20 K) in liquid hydrogen. Specimen thickness for all SENB, SENT, and CT specimens except titanium/room air specimens was approximately $2.5(K_{Ic}/\sigma_{ys})^2$ in. Specimen thickness for SF specimens ranged from $2.5(K_{Ic}/\sigma_{ys})^2$ to $0.25(K_{Ic}/\sigma_{ys})^2$. Relative orientations of crack propagation and rolling directions were identical in all specimens of a given alloy. For aluminum alloy specimens having thicknesses of $2.5(K_{Ic}/\sigma_{ys})^2$, SENB, SENT, and SF specimen tests yielded consistent fracture toughness values at all test temperatures whereas CT specimen tests always yielded lower fracture toughness. For titanium alloy specimens having thicknesses of $2.5(K_{Ic}/\sigma_{ys})^2$, SENB, SENT, CT, and SF specimen tests yielded consistent fracture toughness values at −423 F (20 K); at −320 F (78 K), fracture toughness values from SF specimen tests were significantly greater than those obtained from tests of other specimen types; at 72 F (295 K) no valid fracture toughness data were obtained. Both aluminum alloy SF specimen tests yielded consistent fracture toughness (K_{IE}) values when both flaw depth and distance between flaw tip and back specimen face exceeded $0.5(K_{IE}/\sigma_{ys})^2$.

KEY WORDS: aluminum alloys, titanium alloys, fractures (materials), toughness, fracture strength, bending, tension tests, fracture tests, failure, stresses, cracking (fracturing), cryogenics, liquid hydrogen, liquid nitrogen, aerospace engineering

Nomenclature

K_I Opening mode stress intensity factor

K_{Ic} Plane strain fracture toughness per ASTM E 399 - 70T

[1] Senior specialist engineer, Research and Engineering Division, Aerospace Group, The Boeing Company, Seattle, Wash. 98124.

K_{IE} Plane strain fracture toughness determined from tests of surface flawed specimens

K_Q Apparent plane strain fracture toughness determined from specimens not meeting all ASTM E 399 - 70T requirements

a Crack length in through cracked specimens or crack depth in surface flawed specimens

$2c$ Crack length of surface crack measured at surface of test specimen

σ_{ys} Uniaxial 0.2 percent offset yield strength

Plane strain fracture toughness is receiving increased attention in material selection and design considerations for medium to high strength metallic structures. Considerable plane strain fracture toughness data, obtained from tests of surface flawed specimens [1–5] exist, since the surface flawed specimen is the best available model of potential failure origins in aerospace pressure vessels. However, a recently proposed ASTM test method [6] for plane strain fracture toughness (K_{Ic}) testing of metallic materials covers tests of only single-edge notched bend and compact tension specimens. To assess the applicability of such tests to calculations of relationships between flaw size and failure stress for aerospace hardware, a systematic comparison of plane strain fracture toughness data obtained from tests of through cracked and surface flawed specimens was undertaken. To this end, duplicate 2219-T87 aluminum and 5Al-2.5Sn ELI titanium alloy single-edge notched bend (SENB), single-edge notched tension (SENT), compact tension (CT), and surface flawed (SF) specimens were fractured at 72 F (295 K) in room air, −320 F (78 K) in liquid nitrogen, and −423 F (20 K) in liquid hydrogen, as summarized in the upper part of Table 1.

The proposed ASTM test method specifies minimum specimen thicknesses and crack lengths required to obtain acceptable K_{Ic} values from tests of SENB and CT specimens. To evaluate similar requirements for SF specimens, tests of 2219-T87 aluminum and 5Al-2.5Sn ELI titanium SF specimens were undertaken in which specimen thickness and flaw shape were varied as summarized in the lower part of Table 1. For each alloy, four specimen thicknesses and two flaw shapes were used such that flaw depth to thickness ratios were less than 50 percent for all but the thinnest specimens. Aluminum alloy specimens were tested at 72 F (295 K), −320 F (78 K), and −423 F (20 K). Titanium alloy specimens were tested at −320 F (78 K) and −423 F (20 K).

Relationships between stress intensity, crack size, and nominal stress field have been determined for each of the specimen configurations tested in this program. Stress intensities for SENB, SENT, and CT specimens have been derived using boundary collocation techniques [7–9] and results are summarized in Fig. 1. An approximate stress intensity expression for SF specimens [10] has been derived using a three-dimensional elasticity

TABLE 1—*Test program.*

Purpose	Material	Parent Plate Thickness, in.	Specimen Type	Approximate Specimen Thickness $\times (\sigma_{ys}/K_{Ic})^2$, in.	Surface Flaw Parameters		Number of Tests at		
					$a/2c$	a/t	72 F	−320 F	−423 F
Specimen Configuration Effect Tests	2219-T87 aluminum....	2.50	SENB	2.50	...	...	2	2	2
			SENT		...	...	2	2	2
			CT		...	...	2	2	2
			SF		0.25	0.3	2	2	2
			SF		0.40	0.5	2	2	2
	5Al-2.5Sn ELI titanium.....	0.80	SENB	2.50	...	...	2	2	2
			SENT		...	...	2	2	2
			CT		...	...	2	2	2
			SF		0.25	0.4	2	2	2
			SF		0.40	0.5	2	2	2

Surface Flawed Specimen Thickness Effect Tests	2219-T87 aluminum....	1.00	SF	1.88	0.10	0.4	2	2	2
					0.25	0.5	2	2	2
				1.25	0.10	0.4	2	2	2
					0.25	0.5	2	2	2
				0.63	0.10	0.4	2	2	2
					0.25	0.5	2	2	2
				0.31	0.10	0.7	2	2	2
					0.25	0.8	2	2	2
	5Al-2.5Sn ELI titanium.....	0.375	SF	1.88	0.10	0.4	None	2	2
					0.25	0.5		2	2
				1.25	0.10	0.4		2	2
					0.25	0.5		2	2
				0.63	0.10	0.4		2	2
					0.25	0.5		2	2
				0.31	0.10	0.7		2	2
					0.25	0.8		2	2

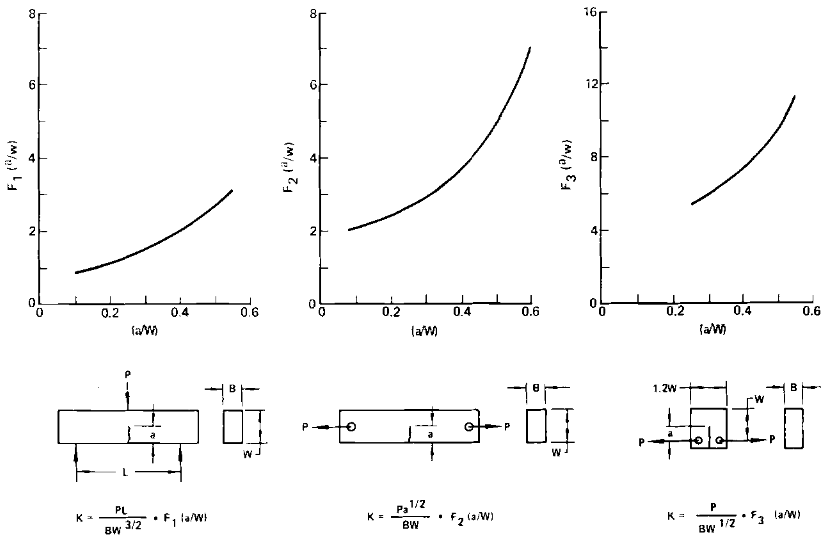

FIG. 1—*Stress intensity expressions for SENB, SENT, and CT specimens.*

solution [11] for elliptical cracks in infinite bodies. The maximum value of stress intensity for the semielliptical surface crack occurs at the end of the semiminor axis of the crack and is given by the expression

$$K_{\mathrm{I}} = 1.1\sigma\sqrt{\pi a/Q} \quad (1)$$

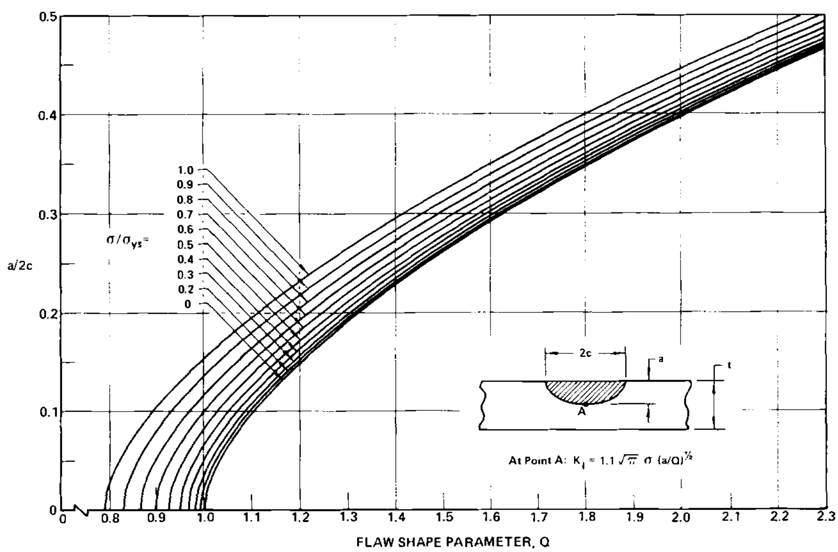

FIG. 2—*Shape parameter curves for surface flaws.*

where σ is a uniform tensile stress acting perpendicular to the plane of the crack and a and Q are defined in Fig. 2. Equation 1 was considered to be applicable for elastic stress levels and surface flaws with depth to half-length (a/c) ratios of less than one and depth to plate thickness (a/t) ratios of less than one half. A number of approximate solutions [*12–15*] have been derived for surface flaw stress intensity when flaw depth is greater than 50 percent of the parent plate thickness. Although the solutions have become increasingly sophisticated, there is still an unknown degree of uncertainty in calculations of stress intensity for surface flaws when a/t exceeds 50 percent.

Materials

Aluminum alloy specimens were machined from 1.0-in. (2.54-cm) and 2.5-in. (6.35-cm)-thick 2219-T87 plate stock. Chemical composition and mechanical properties are given in Tables 2 and 3, respectively.

Titanium alloy specimens were machined from 0.38-in. (0.97-cm) and 0.80-in. (2.03-cm)-thick 5Al-2.5Sn ELI annealed titanium plate stock. Ingot composition is given in Table 2. The plates were obtained in the mill annealed condition after a treatment of 1500 F (1089 K), 0.5 h, air cool. The mill annealed plates showed some evidence of incomplete annealing, so they were reannealed in an argon atmosphere within enclosed retorts using a 1550 F (1117 K), 8-h (0.38-in.-thick plates) or 16-h (0.80-in.-thick plates), retort cool treatment; the resultant mechanical properties are given in Table 3.

TABLE 2—*Chemical composition of materials.*

Element, wt % (except as noted)	2219-T87 Aluminum Plate		5Al-2.5Sn ELI Titanium Plate, Heat No. 294327
	Min	Max	
Copper	5.80	6.80	...
Silicon	...	0.20	...
Manganese	0.20	0.40	...
Magnesium	...	0.02	0.01
Iron	...	0.30	0.19
Chromium	...	...	...
Zinc	...	0.10	...
Vanadium	0.05	0.15	...
Tin	...	...	2.50
Carbon	...	...	0.02
Nitrogen	...	...	70 ppm
Oxygen	...	...	940 ppm
Hydrogen	...	...	94 ppm
Zirconium	0.10	0.25	...
Other elements each	...	...	...
Other elements total	...	...	...
Titanium	0.10	0.20	Bal
Aluminum	Bal	Bal	5.10

TABLE 3—*Mechanical properties of materials.*

Material	Annealing Treatment	Thickness, in.	Test Temperature, deg F	Loading Direction, L = Longitudinal T = Transverse	Ultimate Tensile Strength, ksi	0.2% Offset Yield Strength, ksi	Elongation in 2.0-in. Gage Length, %
5Al-2.5Sn ELI titanium plate....	1550 F/16 h	0.80	72	L	114	108	14
			−320	L	176	173	8
			−423	L	201	187	3
	1550 F/8 h	0.38	72	L	119	114	14
			−320	L	190	179	9
			−423	L	209	196	5
	1500 F/0.5 h	0.38	72	L	122	113	15
			−320	L	187	180	8
			−423	L	222	206	6
2219-T87 aluminum plate...	None	2.50	72	L	69	57	12
				T	69	55	10
			−320	L	87	70	12
				T	86	67	11
			−423	L	105	74	11
				T	101	73	10
		1.00	72	T	69	56	8
			−320	T	86	66	12
			−423	T	100	69	11

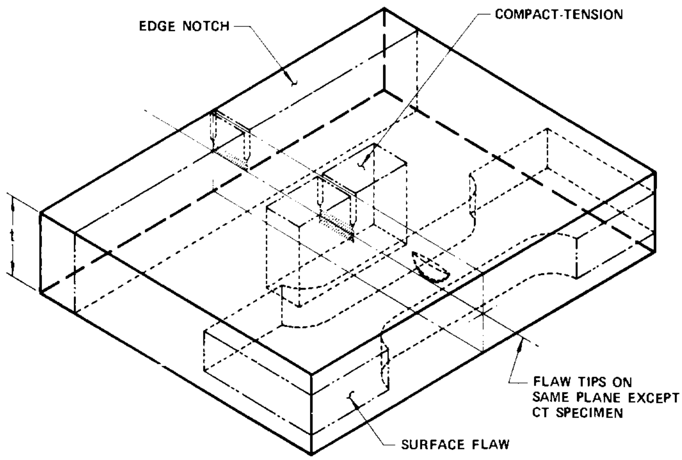

FIG. 3—*Specimen location within plate.*

Procedures

Specimen Configuration Effect Tests

All specimens were cut from either one 2.5-in. (6.35-cm)-thick 2219-T87 aluminum alloy plate or one 0.80-in. (2.03-cm)-thick 5Al-2.5Sn ELI titanium alloy plate as illustrated in Fig. 3. Orientation of crack plane with respect to rolling direction was the same in all specimens of a given alloy, namely, parallel to the rolling direction for the aluminum alloy and perpendicular to the rolling direction for the titanium alloy. The tips of all cracks in SENB, SENT, and SF specimens were located close to the midplane of the parent plate. Crack tips in CT specimens were, respectively, 0.35 in. (0.89 cm) and 0.075 in. (0.19 cm) away from midplane of the aluminum and the titanium alloy parent plates.

Specimen details for SENB, SENT, and CT specimens are shown in Fig. 4. All specimens were fabricated with the largest depth (W) dimensions that could be obtained from the parent plates, namely, 2.50 in. (6.35 cm) for the aluminum specimens and 0.75 in. (1.91 cm) for the titanium specimens. Specimen thicknesses were 1.25 in. (3.18 cm) and 0.40 in. (1.02 cm) for aluminum and titanium specimens, respectively. Thicknesses were chosen to exceed estimated values of $2.5(K_{Ic}/\sigma_{ys})^2$ for all material/environment combinations except titanium/air. For the titanium/air tests, it was estimated that $2.5(K_{Ic}/\sigma_{ys})^2$ exceeded 2.5 in. (6.35 cm), and specimens sufficiently large to measure K_{Ic} could not be machined from the available 0.80-in. (2.03-cm)-thick plate. Loading pinhole locations in the CT specimens were smaller and more widely separated than the hole locations recommended in the ASTM proposed method, since the CT specimens were

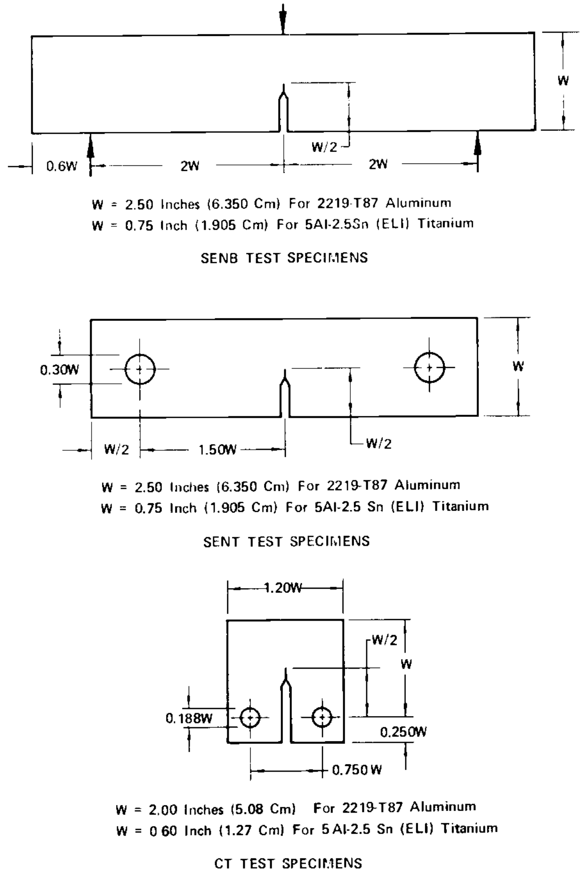

FIG. 4—*Details of SENB, SENT, and CT specimens.*

designed prior to its release. However, CT specimen proportions agreed with Ref *6* requirements in all other respects.

Surface flawed specimen details are summarized in Fig. 5. Specimen thickness was selected to be greater than estimated values of $2.5(K_{IE}/\sigma_{ys})^2$, where K_{IE} is the fracture toughness resulting from the SF specimen tests.

Specimens were precracked by growing fatigue cracks from starter slots, whose details in the SENB, SENT, and CT specimens are summarized in Fig. 6. An electrical discharge machine (EDM) was used to produce a sharp tip at the end of a milled slot. For the aluminum alloy, starter slots fell within the required envelope specified in the method; for the titanium alloy, the 0.01-in. (0.25-cm) milled slot was wider than the maximum allowable value of $0.05W$ (0.038 in. or 0.096 cm). In SF specimens, starter slots were produced by an EDM machine and 0.06-in. (0.15-cm)-thick circular electrodes; electrode tips were machined to a radius of about 0.003 in. (0.008 cm) and an included angle of less than 20 deg.

All specimens were cracked under tension-tension fatigue at 72 F (295 K) in room air. The ratio of maximum cyclic stress intensity to Young's modulus (K_f/E) was less than 0.0012 in.$^{1/2}$ (0.0019 cm$^{1/2}$) for all but the titanium alloy SENB specimens tested at -320 F (78 K) and titanium alloy CT specimens tested at -423 F (20 K), for which K_f/E was 0.0014 in.$^{1/2}$ (0.0022 cm$^{1/2}$). The resulting fatigue cracks in SENB, SENT, and CT specimens were nearly uniform across the specimen width and were approximately 0.10 in. (0.25 cm) long. Fatigue cracks in SF specimens were about 0.04 in. (0.10 cm) and 0.02 in. (0.05 cm) long in the aluminum and titanium alloy specimens, respectively, and the crack peripheries approximated semiellipses.

Tests at 72 F (295 K) were conducted within an enclosed, air conditioned laboratory. Relative humidity was neither controlled nor measured. Tests at -320 F (78 K) and -423 F (20 K) were conducted with test specimens completely submerged in liquid nitrogen and liquid hydrogen, respectively. Specimens were soaked for 15 min prior to loading to stabilize test condi-

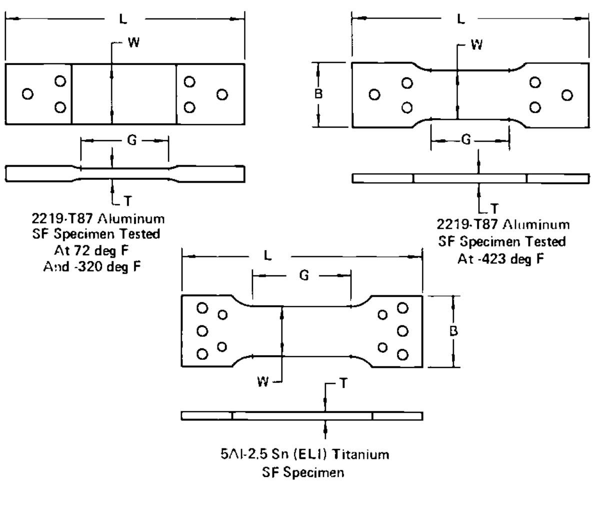

MATERIAL	TEST TEMPERATURE		L		B		W		G		T	
	deg F	deg C	In	Cm	In	Cm	In	Cm	In	Cm	In	Cm
2219-T87 Aluminum	72	22	24.0	61	6.00	15.2	6.00	15.2	9.00	22.9	1.10	2.79
	-320	-196	24.0	61	6.00	15.2	6.00	15.2	9.00	22.9	1.10	2.79
	-423	-253	24.0	61	6.50	16.5	5.00	12.7	8.00	20.3	1.00	2.54
5Al-2.5 Sn(ELI) Titanium	72 -320 -423		12.0	30.5	3.50	8.9	2.50	6.35	5.00	12.70	0.375	0.952

FIG. 5—*Dimensions for SF specimens used in configuration effect tests.*

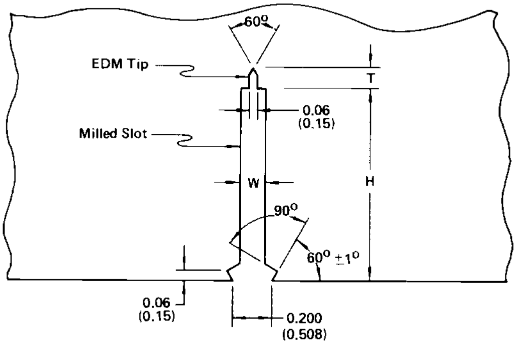

NOTE: Unbracketed Dimensions Are In Inches
Bracketed Dimensions Are In Centimeters

MATERIAL	SPECIMEN TYPE	H		T		W	
		In	Cm	In	Cm	In	Cm
2219-T87 Aluminum	SENB	1.00	2.54	0.10	0.25	0.125	0.318
	SENT	1.00	2.54	0.10	0.25	0.125	0.318
	CT	1.40	3.56	0.10	0.25	0.125	0.318
5Al-2.5 Sn(ELI) Titanium	SENB	0.20	0.51	0.05	0.13	0.100	0.254
	SENT	0.20	0.51	0.05	0.13	0.100	0.254
	CT	0.30	0.76	0.05	0.13	0.100	0.254

FIG. 6—*Crack starter details for SENB, SENT, and CT specimens.*

tions. All specimens were tested in standard test machines. SENB specimens were supported on lightly greased rollers separated by a fixed span.

Continuous recordings of crack opening displacement versus load were obtained in all of the tests except those of SF specimens tested at −423 F (20 K). Crack displacements were measured with a clip gage spring loaded against integrally machined knife edges. Knife edge details for all specimens are shown in Fig. 6. The knife edges of SF specimens were machined into the specimen surface at the mouth of the surface crack. One such knife edge appears as a small rectangle within the dark colored EDM slot on the fracture face of the aluminum alloy SF specimen pictured in Fig. 7. Clip gage details corresponded to those given in Ref *6*, and both the clip gage and the load cell were connected to an X-Y recorder to obtain the test records.

Fracture toughness values for SENB, SENT, and CT specimens were calculated using the equations summarized in Fig. 1. Loads used in the calculations were obtained by drawing secant lines through the origin of each crack opening displacement versus load record having a slope 5 percent less than the slope of the initial straight line part of the test record. The load corresponding to the intersection of secant offset and test record was designated as P_Q and was substituted into the equations in Fig. 1 to calculate fracture toughness.

Fracture toughness values for SF specimens were calculated by substituting maximum applied gross stress and initial flaw dimensions into Eq 1. This procedure implies that fracture originates at the point of maximum

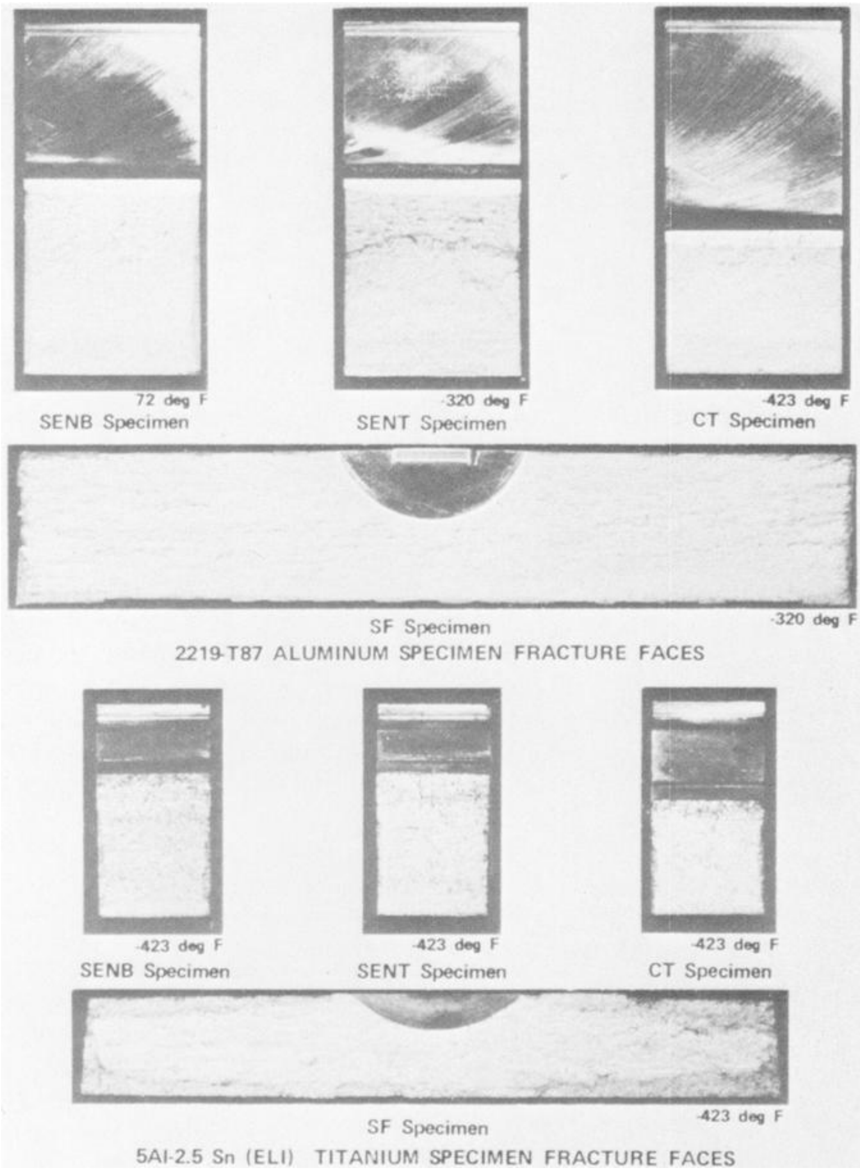

FIG. 7—*Fracture faces of test specimens.*

flaw depth and that unstable flaw propagation is preceded by negligible amounts of slow crack propagation. This implication is discussed in light of the test results in the Results and Discussion section.

Specimen Thickness Effect Tests

All specimens were taken from either 1.0-in. (2.54-cm)-thick 2219-T87 aluminum or 0.38-in. (0.97-cm)-thick 5Al-2.5Sn ELI titanium plate stock. Specimen configurations (but not dimensions) were the same as those given in Fig. 5. A minimum value of 3.5 for the specimen width to crack length ratio was used in the design of all specimens. Crack planes were parallel to the rolling direction in aluminum alloy specimens and perpendicular to the rolling direction in titanium alloy specimens. All specimens were precracked and tested with the same procedures that were followed in the specimen configuration effects tests except that crack opening displacement versus load records were not obtained.

Results and Discussion

Specimen Configuration Effect Tests

Plane strain fracture toughness values obtained from tests of SENB, SENT, and CT specimens along with fracture toughness values obtained from SF specimen tests are given as a function of test temperature in Fig. 8 for both 2219-T87 aluminum and 5Al-2.5Sn ELI titanium alloys.

Crack displacement versus load records for all SENB, SENT, and CT specimens (with the exception of the inadequately sized titanium alloy specimens tested at 72 F) indicated a reasonably abrupt onset of unstable crack propagation. The P_Q load was usually slightly less than the maximum load but always greater than loads corresponding to all points on the test record preceding that at P_Q. Deviations from linearity at $0.8P_Q$ were less than 25 percent of comparable deviations measured at P_Q as required for valid test records [*6*].

Crack displacement versus load records for SF specimens exhibited moderate nonlinearity at loads above about 90 percent of the maximum applied loads. It is believed that the nonlinearity observed in these tests was due primarily to small amounts of slow crack extension that preceded rapid crack propagation. Unreported tests of 2219-T87 aluminum and 5Al-2.5Sn ELI titanium SF specimens conducted at Boeing have shown that moderate amounts of slow crack extension do occur when such specimens are loaded to stress intensity levels near K_{IE} and then unloaded immediately prior to failure. Moderate amounts of crack extension in SF specimens at stress intensity levels less than K_{IE} have been previously reported [*2*] for both 2219-T87 aluminum and 5Al-2.5Sn ELI titanium in environments of room air, liquid nitrogen, and liquid hydrogen.

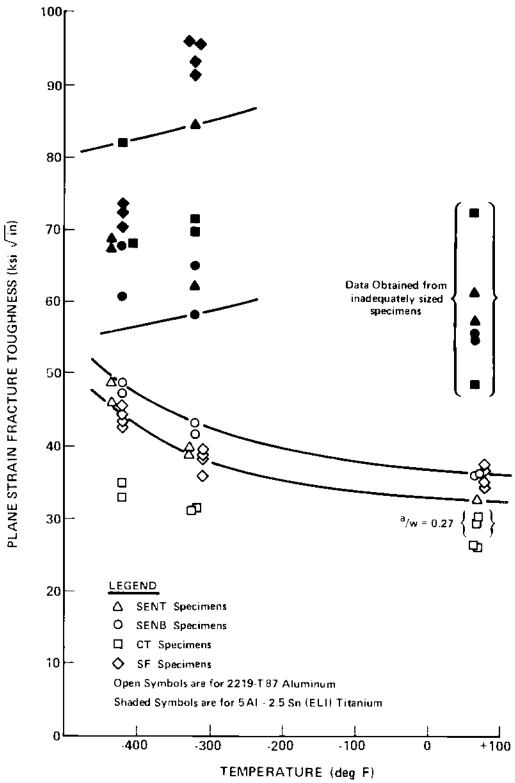

FIG. 8—*Plane strain fracture toughness data for 2219-T87 aluminum and 5Al-2.5Sn ELI titanium.*

Plane strain fracture toughness data for the 2219-T87 aluminum alloy SENB, SENT, and SF specimens are in good agreement, as illustrated in the lower part of Fig. 8. The scatterband was drawn for illustrative purposes and includes all SENB and SENT data. The CT data fall consistently below data for the other specimen types. Some small differences between SENB, SENT, and SF data did exist, some of which were temperature independent and others temperature dependent. For example, SENB data were moderately higher than SENT data at all test temperatures. The SENB data also were above SF data at −320 F (78 K) and −423 F (20 K) but agreed closely with SF data at 72 F (295 K). Small variations in fracture toughness data for SENB, SENT, and SF specimens are not surprising; however, the substantial disagreement between the CT data and all other data was unexpected.

Limited efforts to determine possible reasons for the discrepancies noted in the aluminum alloy fracture toughness data were not successful. Since there was a remote possibility that the CT specimens could have been

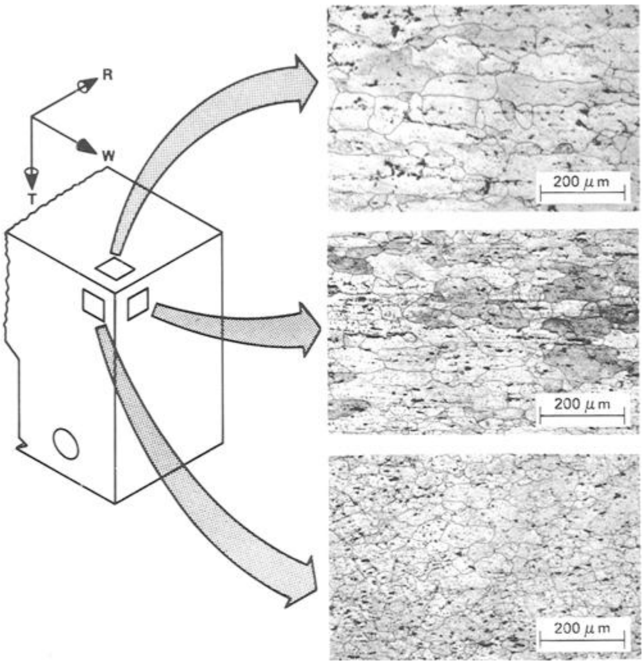

FIG. 9—*Microstructural indications of thickness and rolling direction in 2219-T87 aluminum CT specimens.*

inadvertently fabricated with cracks located in the TR rather than the WT plane, rolling and thickness directions were determined for each CT specimen. The variation of microstructure with direction is illustrated in Fig. 9, which shows that the crack planes were properly oriented in the WT plane of the parent plate.

Two additional CT specimens were tested in room air to determine whether increase in length of ligament between the crack tip and back specimen surface would elevate measured fracture toughness values. To this end, specimens ACL-1 and ACL-2 were fabricated with a crack length to specimen depth (a/W) ratio of 0.27 and an uncracked ligament length of 1.5 in. (3.81 cm) as compared to a/W ratios and ligament lengths of 0.55 and 0.9 in. (2.29 cm) for other CT specimens. The resulting data are plotted in Fig. 8, where it can be seen that the data points were located above those obtained from CT specimens with $a/W \simeq 0.55$ but still below the SENB, SENT, and SF data points. Since crack lengths in specimens ACL-1 and ACL-2 were less than $2.5(K_Q/\sigma_{ys})^2$, it is possible that the increase in fracture toughness values for these specimens was due in part to insufficient crack length rather than increase in uncracked ligament length.

It should also be noted again that diameter and spacing of loading holes in the CT specimens were different from comparable dimensions in specimens used in interlaboratory evaluations of the CT specimen prior to the release of the ASTM method. Since stress intensity in CT specimens is sensitive to boundary conditions, there is a possibility that the loading method used in these tests did not satisfy the boundary conditions assumed in the stress intensity analyses of the CT specimen. At this time, discrepancies noted in the test program between K_{Ic} values obtained from tests of CT specimens and K_{Ic} values obtained from tests of SENB and SENT specimens cannot be explained.

Plane strain fracture toughness data for the 5Al-2.5Sn ELI titanium alloy show a considerable degree of scatter and some disagreement between through cracked and surface cracked specimen data at −320 F (78 K). The scatterband shown in the upper part of Fig. 8 was drawn for illustrative purposes and includes all −423 F (20 K) data and all but the SF data at −320 F (78 K). The SENB, SENT, and CT data indicate little change in fracture toughness between −320 F (78 K) and −423 F (20 K). Other reported SENB data [*16*] have shown a higher toughness at −320 F (78 K) than at −423 F (20 K) for the RT direction. The K_Q values obtained at 72 F (295 K) from inadequately sized specimens are considerably less than previously reported [*1*, *16*] room temperature plane strain fracture toughness values in excess of 100 ksi$\sqrt{\text{in.}}$ (110 MN/m$^{3/2}$). At −423 F (20 K) fracture toughness values for two SENT, one SENB, one CT, and three SF specimens are in good agreement. At −320 F (78 K), the SF data were above the scatterband enclosing the SENT, SENB, and CT data.

It has been suggested that the disagreement between the −320 F (78 K) SF and through cracked specimen data for the 5Al-2.5Sn ELI titanium alloy was due to inadequate crack depths in the SF specimens. In SF specimens both crack depth (a) and distance between the crack tip and back specimen face ($t - a$) must be sufficiently large multiples of $(K_{IE}/\sigma_{ys})^2$ to ensure that K_{IE} is the controlling mechanical parameter in the fracturing process. Data in the following section of this report show that 5Al-2.5Sn ELI titanium SF specimens yield essentially constant values of K_{IE} at −320 F (78 K) and −423 F (20 K) when both a and $t - a$ exceed 0.5 $(K_{IE}/\sigma_{ys})^2$. In the subject tests, a and $t - a$ values exceeded $0.5(K_{IE}/\sigma_{ys})^2$ in all −320 F (78 K) investigations, so it was concluded that increases in crack depth and specimen dimensions would probably not have resulted in better agreement between the SF and through cracked specimen data for the 5Al-2.5Sn ELI titanium alloy at −320 F (78 K).

The significant change in fracture toughness values between −423 F (20 K) and −320 F (78 K) for the titanium alloy SF specimens suggests that a fracture mode transition may have occurred between the two test temperatures. Other evidence of a change in plane strain fracture behavior in 5Al-2.5Sn ELI titanium alloy between −423 F (20 K) and −320 F (78 K) was reported in Ref *1*, where it was observed that surface flawed cylindrical tanks failed at −320 F (78 K) by splitting open, whereas tanks

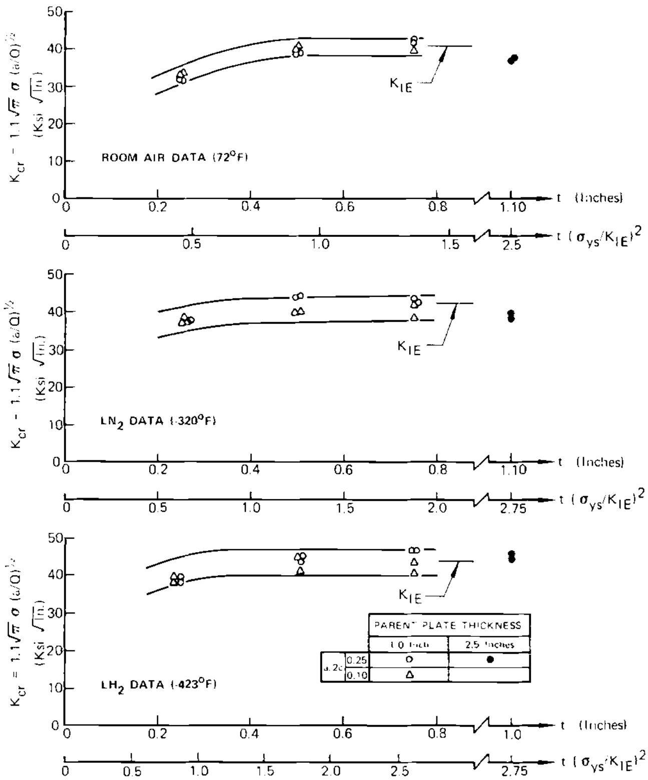

FIG. 10—*Fracture data for 2219-T87 aluminum base metal (varied thickness surface flawed specimen tests).*

failed at −423 F (20 K) by completely shattering the vessel. It was also noted that areas of fatigue induced flaw growth in 5Al-2.5Sn ELI surface flawed specimens and cylindrical tanks were characterized by fatigue striations at −320 F (78 K) but were completely devoid of striations at −423 F (20 K). In contrast to SF specimens, through-the-thickness cracked specimens yielded no evidence of differences in fracture behavior between −423 F (20 K) and −320 F (78 K). Since the crack planes in all through cracked specimens were subjected to significant bending stresses whereas crack planes in SF specimens are subjected primarily to tensile stresses, there is a possibility that differences in titanium alloy −320 F (78 K) fracture toughness data are related to bending stresses. To date, no effort has been made to evaluate this possibility.

Surface Flawed Specimen Thickness Effects

Fracture data for 2219-T87 aluminum and 5Al-2.5Sn ELI titanium alloy SF specimens of varied thickness are plotted in Figs. 10 and 11, respectively. Data are plotted for all tests in which flaw depth to specimen thickness ratios were less than one half. Apparent fracture toughness (K_{cr}) values were calculated by substituting gross failure stress and initial flaw parameters into Eq 1 and plotted as a function of specimen thickness. Specimen thickness is given both in inches and in multiples of $(K_{IE}/\sigma_{ys})^2$, where K_{IE} is the average fracture toughness value obtained from the thickest test specimens. For purposes of comparison, data obtained from surface flawed specimens tested in the specimen configuration effect tests are represented in Figs. 10 and 11 by solid circles. The data plots show that consistent fracture toughness values were obtained for all material/environment combinations from specimens thicker than about $1.0(K_{IE}/\sigma_{ys})^2$.

Flaw growth prior to specimen fracture was observed during room temperature tests of the thinnest surface flawed specimens. In 0.125-in.

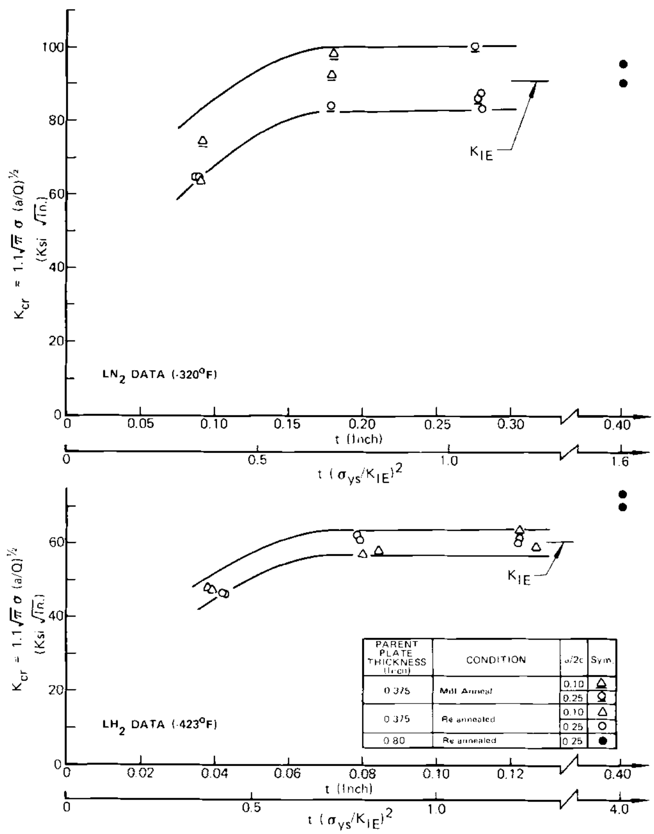

FIG. 11—*Fracture data for 5Al-2.5Sn ELI titanium base metal (varied thickness surface flawed specimen tests).*

(0.318-cm)-thick aluminum specimens containing flaws with $a/2c = 0.25$ and $a/t = 0.8$, the flaws were observed to grow through the specimen thickness prior to the onset of unstable flaw propagation. In one specimen, the flaw penetrated the specimen thickness at a gross stress level of 46.5 ksi (320.6 MN/m^2). Applied load was then held constant for 5 min while the flaw was observed through a magnifying glass. No flaw growth could be detected under constant load. The load was then increased, until the specimen failed at 50.5 ksi (348.2 MN/m^2). In a second specimen, the flaw penetrated the specimen thickness at a gross stress level of 50.9 ksi (351.0 MN/m^2). The stress was then held constant for 20 s, at which time the specimen failed. In 0.125-in. (0.318-cm)-thick aluminum specimens containing flaws with $a/2c = 0.10$ and $a/t = 0.70$, a slight amount of dimpling was observed on the back specimen face opposite the flaw tip; however, the flaw did not penetrate the specimen thickness prior to failure.

Specimens tested at −320 F (78 K) and −423 F (20 K) were completely submerged in the test media and could not be visually monitored. However, there was indirect evidence that flaws in the 0.02-in. (0.051-cm)-thick titanium specimens tested at −423 F (20 K) grew through the specimen thickness at loads less than the fracture load. While loading at a constant rate of head travel, a reasonably abrupt interruption in the rate of load increase was noted at a load less than the failure load, after which the test specimen became more compliant. The observed change in load rate behavior probably occurred when the flaw grew through the specimen thickness. Other −423 F (20 K) test data have been published [*3*] for 0.02-in. (0.051-cm)-thick 5Al-2.5Sn ELI titanium surface flawed specimens that indicate that surface flaws deeper than 60 percent of the specimen thickness can be expected to grow through the specimen thickness at loads less than the failure load.

The effect of flaw shape on K_{IE} values was small. There was a slight tendency for specimens containing flaws with $a/2c = 0.10$ to yield smaller K_{IE} values than specimens containing flaws with $a/2c = 0.25$. This trend is in agreement with a recent stress intensity analysis for surface flawed specimens [*15*] which shows that for constant a/t the ratio of applied stress intensity to load increases moderately for decreasing $a/2c$. Since Eq 1 does not account for this effect, there appeared to be a slight effect of $a/2c$ on K_{IE} values in the test results.

The data in Figs. 10 and 11 can be used to draw some conclusions with respect to crack depth and specimen thickness requirements for 2219-T87 aluminum and 5Al-2.5Sn ELI titanium surface flawed specimens. Most of the data were developed by testing specimens with $a/t \simeq 0.5$. Since consistent fracture toughness values were obtained for specimens thicker than about $1.0(K_{IE}/\sigma_{ys})^2$, it is concluded that a characteristic fracture toughness value (K_{IE}) can be used to predict fracture strength of surface flawed structures for which both crack depth and depth of ligament between the flaw tip and back specimen face are greater than $0.5(K_{IE}/\sigma_{ys})^2$. In four of the five material/environment combinations tested, the characteristic fracture toughness had a numerical value that was in agreement with the K_{Ic} values determined according to the ASTM method requirements. The excepted material/environment combination is 5Al-2.5Sn ELI titanium/liquid nitrogen, for which the K_{Ic} values were less than the K_{IE} values determined from SF tests.

Summary and Recommendation

This experimental program provides the first comparison between plane strain fracture toughness data obtained from tests of both surface flawed and through cracked fracture specimens for a single direction of crack propagation. Good agreement was obtained between fracture toughness data derived from tests of 2219-T87 aluminum surface flawed (SF), single-edge notched bend (SENB), and single-edge notched tension (SENT) specimens at 72 F (295 K), −320 F (78 K), and −423 F (20 K). However, fracture toughness values derived from tests of 2219-T87 aluminum compact tension (CT) specimens were consistently lower than the other aluminum alloy data. Similar tests of 5Al-2.5Sn ELI titanium SF, SENB, SENT, and CT specimens yielded fracture toughness data that showed reasonable agreement at −423 F (20 K); however, at −320 F (78 K), fracture toughness values from tests of SF specimens were higher than values obtained from tests of SENB, SENT, and CT specimens.

Fracture tests of 2219-T87 aluminum and 5Al-2.5Sn ELI titanium SF specimens in which specimen thickness was varied yielded consistent fracture toughness values for specimens in which both flaw depth and distance between the flaw tip and back specimen face exceeded $0.5(K_{IE}/\sigma_{ys})^2$ and flaw depth was approximately 50 percent of the specimen thickness. The fracture toughness values were in good agreement with plane strain fracture toughness data determined from tests of SENB and SENT specimens for 2219-T87 aluminum at 72 F (295 K), −320 F (78 K), and −423 F (20 K) and from tests of SENB, SENT, and CT specimens for 5Al-2.5Sn ELI titanium tested at −423 F (20 K). For 5Al-2.5Sn ELI titanium at −320 F (78 K) fracture toughness values from tests of SF specimens were greater than plane strain fracture toughness values determined from tests of SENB, SENT, and CT specimens.

The tests show that fracture toughness values from tests of specimens designed to yield plane strain fracture toughness can vary with specimen configuration. Consequently, it is recommended that fracture toughness data for use in design applications be developed using specimen configurations that simulate potential failure origins. For example, part-through cracks are best simulated by surface flawed specimens and through-the-thickness cracks by specimens containing through-the-thickness cracks.

Acknowledgments

I wish to acknowledge the invaluable help of R. W. Finger and A. A. Ottlyk who coordinated and conducted the tests performed in this program. This work was sponsored by the NASA Lewis Research Center under the direction of Gordon T. Smith.

References

[1] Tiffany, C. F., Lorenz, P. M., and Hall, L. R., "Investigation of Plane Strain Flaw Growth in Thick-Walled Tanks," NASA CR-54837, National Aeronautics and Space Administration, Feb. 1966.

[2] Tiffany, C. F., Lorenz, P. M., and Shah, R. C., "Extended Loading of Cryogenic Tanks," NASA CR-72252, National Aeronautics and Space Administration, July 1967.

[3] Masters, J. N., Haese, W. P., and Finger, R. W., "Investigation of Deep Flaws in Thin Walled Tanks," NASA CR-72606, National Aeronautics and Space Administration, Dec. 1969.

[4] Hall, L. R., "Plane Strain Cyclic Flaw Growth in 2014-T62 Aluminum and 6Al-4V(ELI) Titanium," NASA CR-72396, National Aeronautics and Space Administration, Nov. 1968.

[5] Randall, P. N., "Severity of Natural Flaws as Fracture Origins, and a Study of the Surface-Cracked Specimen," AFML-TR-66-204, Air Force Materials Laboratory, Aug. 1966.

[6] ASTM Committee E-24, Proposed Method of Test for Plane Strain Fracture Toughness of Metallic Materials, *Annual Book of ASTM Standards*, Part 31, May 1969, pp. 1099–1114 (to be approved).

[7] Gross, B., Srawley, J. E., and Brown, W. F., Jr., "Stress-Intensity Factors for a Single-Edge-Notch Tension Specimen by Boundary Collocation of a Stress Function," Technical Note D-2395, National Aeronautics and Space Administration, Aug. 1964.

[8] Gross, B. and Srawley, J. E., "Stress-Intensity Factors for Single Edge Notch Specimens in Bending or Combined Bending and Tension by Boundary Collocation of a Stress Function," Technical Note D-2603, National Aeronautics and Space Administration, Jan. 1965.

[9] Gross, B. and Srawley, J. E., "Stress Intensity Factors for Three Point Bend Specimens by Boundary Collocation," Technical Note D-3092, National Aeronautics and Space Administration, Dec. 1965.

[10] Irwin, G. R., *Journal of Applied Mechanics, ASME Transactions*, Series E, JAMCA, Vol. 29, Vol. 84, Dec. 1962.

[11] Green, A. E. and Sneddon, I. N., *Proceedings of the Cambridge Philosophical Society*, PCPSA, Vol. 46, 1959.

[12] Paris, P. C. and Sih, G. C. M. in *Symposium on Fracture Toughness Testing and Its Applications, ASTM STP 381*, American Society for Testing and Materials, April 1965, p. 51.

[13] Kobayashi, A. S., "On the Magnification Factors of Deep Surface Flaws," Structural Development Research Memorandum No. 16, Research Division, Aerospace Group, The Boeing Company, Dec. 1965.

[14] Smith, F. W., "Stress Intensity Factors for a Semi-Elliptical Flaw," Structural Development Research Memorandum No. 17, Research Division, Aerospace Group, The Boeing Company, Aug. 1966.

[15] Kobayashi, A. S. and Moss, W. L., "Stress Intensity Magnification Factors for Surface-Flawed Tension Plate and Notched Round Tension Bar," Proceedings of Second International Conference on Fracture, Brighton, England, 1969.

[16] Pyle, R., Schillinger, D. E., and Carman, C. M., "Plane Strain Fracture Toughness and Mechanical Properties of 2219-T87 Aluminum and 5Al-2.5Sn(ELI) Titanium Alloy Weldments and One-Inch-Thick 5Al-2.5Sn(ELI) Titanium Alloy Plate," NASA-CR-72154, National Aeronautics and Space Administration, Washington, D. C., 1968.

T. W. Orange,[1] *T. L. Sullivan,*[1] *and F. D. Calfo*[1]

Fracture of Thin Sections Containing Through and Part-through Cracks

REFERENCE: Orange, T. W., Sullivan, T. L., and Calfo, F. D., **"Fracture of Thin Sections Containing Through and Part-through Cracks"** *Fracture Toughness Testing at Cryogenic Temperatures, ASTM STP 496*, American Society for Testing and Materials, 1971, pp. 61–81.

ABSTRACT: Current fracture mechanics theory is used to illustrate the effects of crack dimensions and material properties on fracture stresses for through-thickness and part-through cracks. The implication of the analysis for leak-before-burst design of pressure vessels is discussed.

The applicability of plane strain theory to surface cracks in thin metal sections was studied experimentally. Specimens containing surface cracks of various depths and lengths and specimens with through cracks in the same range of crack lengths were tested. Ti-5Al-2.5Sn ELI (0.06 and 0.11 in. (1.6 and 2.9 mm) thick), 2014-T6 aluminum (0.06 in. (1.6 mm) thick), and 2219-T87 aluminum (0.07 in. (1.6 mm) thick) were tested at −423 F (20 K); the 2219-T87 alloy was also tested at +70 and −320 F (300 and 77 K).

The fracture tests indicate that, when Irwin's plastic zone size is less than about one tenth of the uncracked ligament depth (thickness minus crack depth), surface crack fracture behavior is in agreement with plane strain theory. When the plastic zone is greater than the ligament depth, fracture stresses for surface crack specimens are nearly the same as for specimens with through cracks of the same original length.

KEY WORDS: fracture mechanics, fracture strength, cracking (fracturing), aluminum alloys, titanium alloys, plastic properties, crack propagation, strains, stresses, fracture tests, cryogenics

Nomenclature

- a Depth of semielliptical surface crack
- c Half-length of through crack or semielliptical surface crack
- K_c Fracture toughness under mixed mode fracture conditions
- K_{cn} Nominal value of K_c, based on original crack length and final load
- K_{Ic} Opening mode (plane strain) fracture toughness

[1] Aerospace technologists, Structural Materials, Lewis Research Center, National Aeronautics and Space Administration, Cleveland, Ohio 44135.

K_Q Apparent value of K_{Ic}
M Free surface correction factor (magnification factor)
t Plate thickness
W Specimen width
Φ Complete elliptical integral of the second kind for the argument $k^2 = 1 - a^2/c^2$
σ Fracture stress (based on gross area)
σ_{ys} Material yield strength (0.2 percent offset)

Linear elastic fracture mechanics can be used with confidence only for a limited number of practical crack problems at the present time. Some of the uncertainties associated with through crack testing are mentioned in Ref *1* (authors' reply to discussion by R. H. Heyer). Irwin's surface crack fracture analysis [*2*] assumes that conditions of plane strain prevail, and its application is customarily limited to crack depths less than half of the plate thickness. However, in spite of these apparently severe limitations, fracture mechanics theory is still useful. It can provide at least a qualitative description of the effects of material and geometrical parameters on fracture strength. In some cases, as will be shown later, it can also give a good quantitative description.

Current fracture mechanics analysis is based on linear elastic theory. In lieu of an elastoplastic analysis, nonbrittle materials are treated in an approximate manner. Localized yielding at the tip of a crack is accounted for by adding a portion of the plastic zone length to the actual crack length. As long as the plastic zone is small compared to the crack length and specimen dimensions, the approximation has proven useful.

For small-scale yielding, the plastic zone size is proportional to the square of the ratio of stress intensity to yield strength. Thus simple plastic zone corrections should be adequate as long as the crack length and specimen dimensions are greater than some multiple of the square of this ratio. For edge cracked or through cracked specimens, the significant specimen dimensions are considered to be the crack length, uncracked ligament length, and thickness. The proposed American Society for Testing and Materials (ASTM) plane strain toughness test method [*3*] requires that thickness and crack length be greater than $2.5(K_{Ic}/\sigma_{ys})^2$ and implies that the ligament length (width minus crack length) be greater than about $2(K_{Ic}/\sigma_{ys})^2$. These criteria should be sufficiently conservative to apply to all classes of materials. However, for some materials or test specimens or both (for example, see Ref *4*) the theory appears applicable (within engineering accuracy) to much smaller cracks as well.

Irwin's analysis for a surface crack in a plate [*2*] assumes that plane strain conditions prevail at fracture and that the crack dimensions are small compared with the plate dimensions. Brown and Srawley ([*1*], pp. 30–33) indicate that the analysis may not be applicable if the crack depth is less than $2.5(K_{Ic}/\sigma_{ys})^2$. Although the concept has not been adequately tested, there should probably be a minimum ligament depth (in this case, plate thickness minus crack depth) requirement also, as there is for the edge cracked specimens. For two reasons (depth-to-thickness limit and minimum ligament depth), then, application of the analysis to material thicknesses much less than $5(K_{Ic}/\sigma_{ys})^2$ cannot be assured.

The analysis of through cracks under mixed mode failure conditions is also uncertain. It is well known that K_c decreases with increasing thickness until it reaches the limiting plane strain value K_{Ic}. As discussed in Ref *5* (pp. 138–143 and 155–158), K_c is not necessarily independent of crack length and specimen width. However, for many materials the form of the crack extension resistance curve (R curve) is such that, for sufficiently large test specimens, K_c is essentially constant [*6*]. It is also possible to calculate a nominal toughness parameter K_{cn} based on final load and original crack length (neglecting subcritical crack growth), but this is less likely to be constant. Although it is unsuitable for component design purposes, as shown by Kuhn [*7*], the concept of a constant K_{cn} is useful for the illustrative examples that follow.

The plastic zone at the crack tip is even less well understood than the subjects just discussed. Different analytical models lead to significantly different estimates of both the size and shape of the plastic zone. When used as corrections to a large crack length, these discrepancies will affect fracture toughness calculations only slightly. But uncertainty regarding the plastic zone size makes it difficult to predict whether or not the plastic zone at the tip of a surface crack will extend completely through the plate thickness prior to failure. As will be shown later, this appears to affect fracture behavior significantly.

Rice [*8*] has discussed various analytical models at length. Hahn and Rosenfield [*9*] have compared observed plastic zones in Fe-3Si steel with several analytical models. They conclude that none of the models completely describe the observed plastic zones, which were somewhat "butterfly shaped." Lacking an exact description, a lower bound on the plastic zone size is still possible. The results of Ref *9* suggest that the extent of the plastic zone (projected onto the crack plane) is roughly twice Irwin's [*2*] plastic zone size term, in the absence of large-scale yielding and nearby stress-free surfaces. Thus, if the uncracked ligament behind a surface crack is less than twice Irwin's plastic zone size, one can be almost certain that the plastic zone has actually spread completely through the thickness. Note that, if the plastic zone at the tip of a crack is butterfly shaped, it might (under rising load) first reach the back surface at points out of the crack plane, as in Fig. 1 (taken from Ref *10*).

In this paper fracture mechanics analysis is used to predict the effects of crack dimensions and material properties on fracture stress for through cracks and part-through surface cracks. Fracture specimens with through

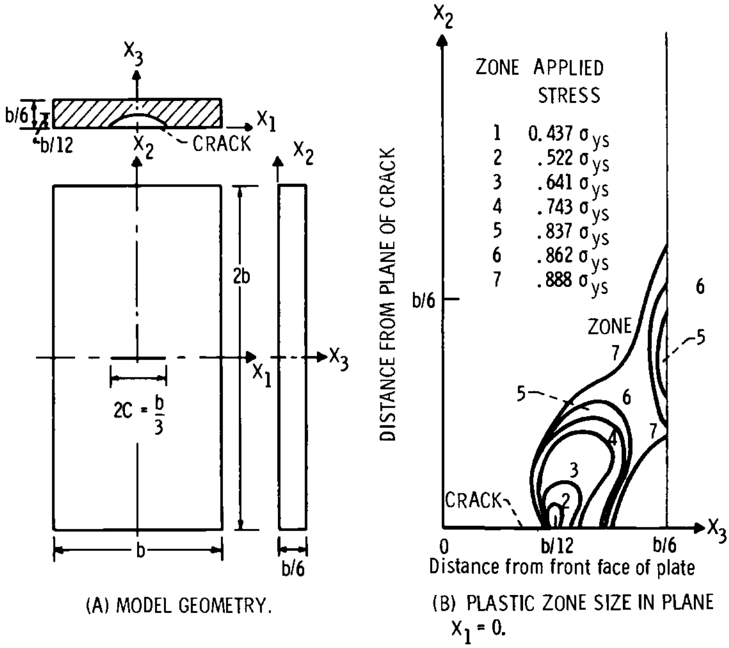

FIG. 1—*Specimen plastic zone* (*Ref* 10).

cracks and with surface cracks were tested at cryogenic temperatures. The results are compared with the predicted trends.

Analysis

Effects of Crack Geometry

Even though its application to design problems is restricted, current fracture mechanics theory can be used to illustrate the effects of crack geometry and material properties on fracture strength and fracture behavior. For the sake of discussion, assume that through cracks are governed by plane stress conditions and surface cracks by plane strain.

Fracture stresses for through-thickness cracks [1] and for surface cracks [2] in a wide, flat plate can be written as

$$\sigma_{\mathrm{thru}} = K_c \Big/ \sqrt{\frac{\pi}{2}\, 2c + \frac{1}{2}\left(\frac{K_c}{\sigma_{ys}}\right)^2} \quad \text{(1a)}$$

$$\sigma_{\mathrm{surf}} = K_{Ic} \Big/ \frac{M}{\Phi}\sqrt{\pi a + \frac{1}{4\sqrt{2}}\left(\frac{K_{Ic}}{\sigma_{ys}}\right)^2} \quad \text{(1b)}$$

where Φ is a function of crack shape and M is a free surface correction factor (taken by Irwin to be ~1.1 for crack depths less than half thickness).

The correction factor of Kobayashi and Moss (denoted as M_e in Ref *11*) was used (rather than Irwin's) so that cracks deeper than half thickness might be considered in this paper. For the reader's convenience, a plot of M/Φ is included as Fig. 2.

For purposes of illustration, it is appropriate (as discussed by Irwin and Srawley [*12*]) to consider the case where $t = K_c^2/2\pi\sigma_{ys}^2$. The previous equations can then be written (for this thickness only) as

$$\frac{\sigma_{\text{thru}}}{\sigma_{ys}} = \sqrt{2}\left(\frac{1}{2}\frac{2c}{t} + 1\right)^{-1/2} \qquad \text{(2a)}$$

$$\frac{\sigma_{\text{surf}}}{\sigma_{ys}} = \sqrt{2}\frac{K_{Ic}}{K_c}\frac{\Phi}{M}\left[\frac{a}{t} + \frac{1}{2\sqrt{2}}\left(\frac{K_{Ic}}{K_c}\right)^2\right]^{-1/2} \qquad \text{(2b)}$$

These equations are plotted in Fig. 3 for the case where $K_{Ic} = 0.5K_c$. Equation 2*b* is plotted for constant crack shape ($a/2c$) as well as for constant depth (a/t). The largest depth plotted is that for which the plastic zone is expected to extend completely through the plate thickness at fracture. The applicability of the analysis to deeper cracks is highly questionable. If, as discussed earlier, the actual plastic zone size is taken to be twice

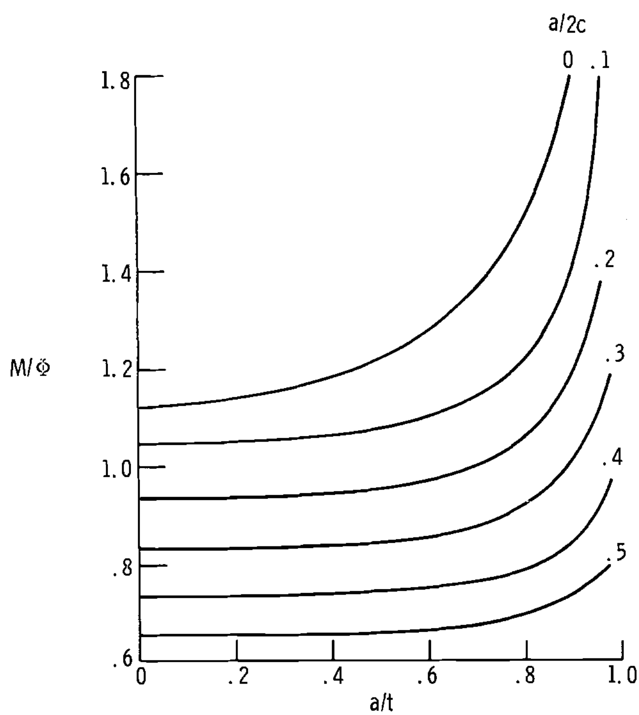

FIG. 2—*Correlation factor used in Eq 2*b.

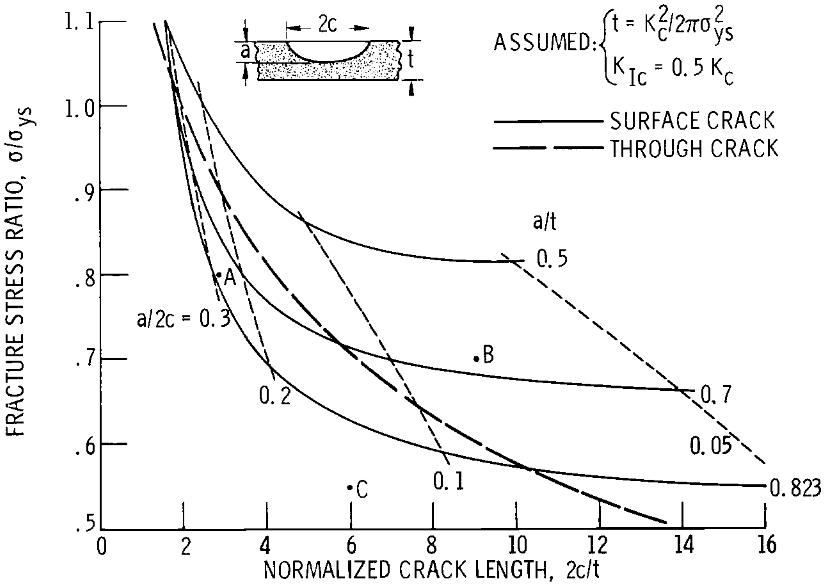

FIG. 3—*Effect of crack geometry on predicted fracture stress for through and part-through cracks.*

Irwin's term, the limiting depth (for this example) is

$$\left(\frac{a}{t}\right)_{max} = 1 - \frac{1}{\sqrt{2}}\left(\frac{K_{Ic}}{K_c}\right)^2 \qquad (3)$$

Figure 3 shows that theoretically a surface crack can fracture (or at least start to fracture) at a lower stress than a through crack of the same length and that this would be most likely to occur for a deep crack with $a/2c$ equal to about 0.2 to 0.3. With the aid of Fig. 3 we can speculate on the effect of crack geometry on the actual fracture process. Consider a surface crack whose geometry is defined by the point A. When the load is increased to $0.8\sigma_{ys}$, the crack should start to propagate rapidly through the thickness with little if any increase in crack length. But the stress required to propagate a through crack of the same length is much greater (about $0.9\sigma_{ys}$); thus, the crack should self-arrest and become a stable through-thickness crack. If the crack were in a pressure vessel, the vessel would leak rather than fail catastrophically.

Consider now a surface crack whose geometry is defined by the point B. When the load is increased to $0.7\sigma_{ys}$, the crack should start to propagate through the thickness. But if there is no load relaxation, the applied stress will be more than sufficient to propagate a through crack of that length and the crack should continue to propagate. A pressure vessel with such a crack would probably fail catastrophically.

For the surface crack defined by point C, the plastic zone would surely grow through the thickness prior to failure, and most of the uncracked ligament would undergo plastic deformation. Under these conditions, fracture might well be controlled by the stress intensity at or near the major axis of the semiellipse. If this crack were in a pressure vessel, elastic theory could not predict whether it would leak or burst. Lacking more powerful analytical methods, we might speculate that, if the crack opening displacement were sufficiently large, the ligament might fail by tensile instability (and the vessel would leak) and that this would be most likely for long cracks. But the yielded ligament might also act as a plastic hinge, allowing the cracked region to bulge outward in the manner associated with through cracks [*13*]. This would induce a bending stress which would further complicate the problem. Under these conditions it would be unwise to expect a cracked tension specimen to simulate the behavior of a cracked pressure vessel.

The empirical relation developed by Eiber et al ([*14*], Fig. 15) for part-through V notches in gas line pipe is similar in appearance to Fig. 3 of this paper. Their burst tests also indicate that failure type (that is, leak or burst) can be correlated with relative fracture stress for through cracks and surface cracks of the same length. If the fracture stress for a given surface crack is less than that for a through crack of the same length, that surface crack will result in a leak at failure; if greater, catastrophic fracture will occur.

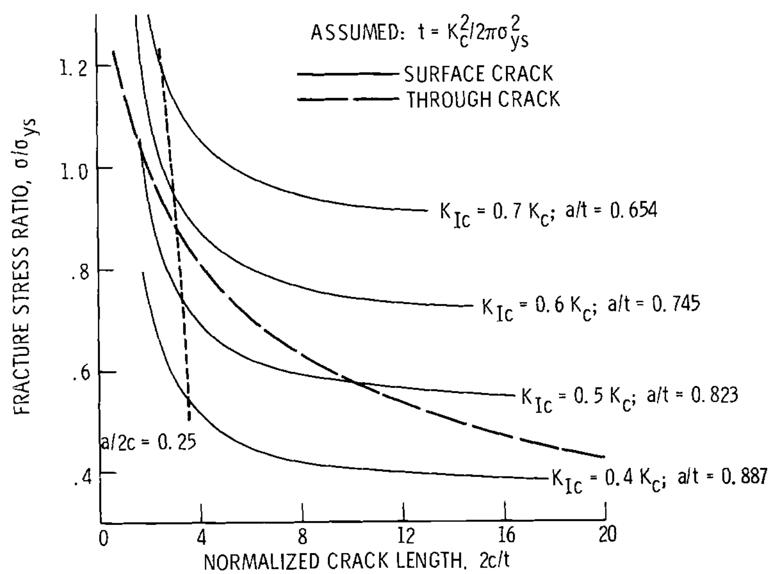

FIG. 4—*Effect of material toughness on predicted fracture stress for through and part-through cracks at limiting depth.*

TABLE 1—*Chemical composition of materials tested (percent by weight).*

Alloy	Al	C	Cr	Cu	Fe	H	Mg	Mn	N	O	Si	Sn	Ti	V	Zn	Zr
Ti-5Al-2.5Sn (0.06 in.)	5.3	0.02	...	...	0.18	0.0040	...	0.01	0.007	0.098	...	2.5	balance	...	...	...
Ti-5Al-2.5Sn (0.11 in.)	5.3	0.02	...	...	0.18	0.0034	...	0.01	0.007	0.091	...	2.5	balance	...	...	...
2014-T6 aluminum	balance	...	0.04	4.45	0.60	0.0005	0.57	0.69	0.0012	0.0005	0.92	...	0.02	...	0.05	...
2219-T87 aluminum	balance	...	...	5.85	0.19	...	0.012	0.25	...	...	0.12	...	0.09	0.08	0.09	0.11

TABLE 2—*Tensile properties of test materials (average: longitudinal direction).*

Alloy	Test Temperature		Yield Strength		Ultimate Strength		Elastic Modulus		Elongation in 2 in. (5 cm), %
	deg F	deg K	ksi	MN/m²	ksi	MN/m²	psi	N/m²	
Ti-5Al-2.5Sn, 0.06 in. (1.6 mm)	+70	300	119	821	129	887	17×10^6	120×10^9	14
	−320	77	193	1330	202	1390	19	130	16
	−423	20	228	1570	247	1710	19	130	13
Ti-5Al-2.5Sn, 0.11 in. (2.9 mm)	+70	300	105	727	114	785	17×10^6	120×10^9	18
	−320	77	178	1230	189	1300	19	130	19
	−423	20	211	1450	223	1540	...[a]	...[a]	...[a]
2014-T6 aluminum	+70	300	65.0	448	72.3	499	10×10^6	72×10^9	...[b]
	−320	77	75.2	519	86.7	598	12	79	...[b]
	−423	20	80.3	554	99.7	687	12	80	...[b]
2219-T87 aluminum	+70	300	55.0	379	67.7	467	11×10^6	74×10^9	11
	−320	77	64.5	445	84.0	579	11	79	12
	−423	20	70.7	487	96.3	664	12	83	14

[a] Measurement considered unreliable.
[b] Not measured.

Effects of Material Properties

The limits of applicability of this analysis are also affected by the material properties. Equation 3 shows that the limiting crack depth (at which the plastic zone just penetrates the thickness) is also a function of the ratio K_{Ic}/K_c. Figure 4 shows the effect of K_{Ic}/K_c at the limiting depth (for this specific thickness). From this figure it appears that leak-before-burst failures cannot be predicted at all if K_{Ic} is greater than about $0.6K_c$ (for this thickness), and they can be expected over a wider range of crack lengths if K_{Ic}/K_c is low. Again, a crack with a depth to length ratio ($a/2c$) of about 0.25 appears to be the one most likely to leak rather than burst at failure.

Experimental Procedure

Materials

The titanium alloy was purchased in two thicknesses rolled from the same heat. Mill analyses for both are given in Table 1. The 2014-T6 aluminum alloy (unclad) was from the same lot used in an earlier study [*6*]. The analysis given was made by a commercial laboratory. The 2219-T87 aluminum alloy (also unclad) was from the same lot studied in Ref *15*; its analysis is also given in Table 1. The tensile properties listed in Table 2 were determined on the standard tension specimen shown in Fig. 5*a* with differential transformer extensometers.

Fracture Specimens

Titanium fracture specimen configurations were as shown in Figs. 5*b* to 5*d*. All 2014-T6 specimens were as shown in Fig. 5*d*. The 2219-T87 specimens, Figs. 5*e* and 5*f*, were sized to be directly comparable with the surface crack specimens tested in Ref *15*.

Natural cracks were grown from crack starters by fatigue cycling the specimens at low stress. Crack starters for all through crack and most surface crack specimens were made by electrical discharge machining. For a few of the 2014-T6 surface crack specimens, sharp surface grooves were machine scribed. All through crack and some surface crack specimens were fatigue sharpened in tension. To obtain more elongated cracks, some surface cracks were extended in cyclic unidirectional bending. For all specimens the nominal net cyclic stress was less than half the material yield strength.

Apparatus and Procedure

The 2219-T87 through crack fracture specimens were fitted with antibuckling guides and tested in a 400,000-lb (1.8-MN)-capacity, screw powered tension testing machine. All other specimens were tested in hydraulic machines having capacities of 20,000, 24,000, and 120,000 lb (89,

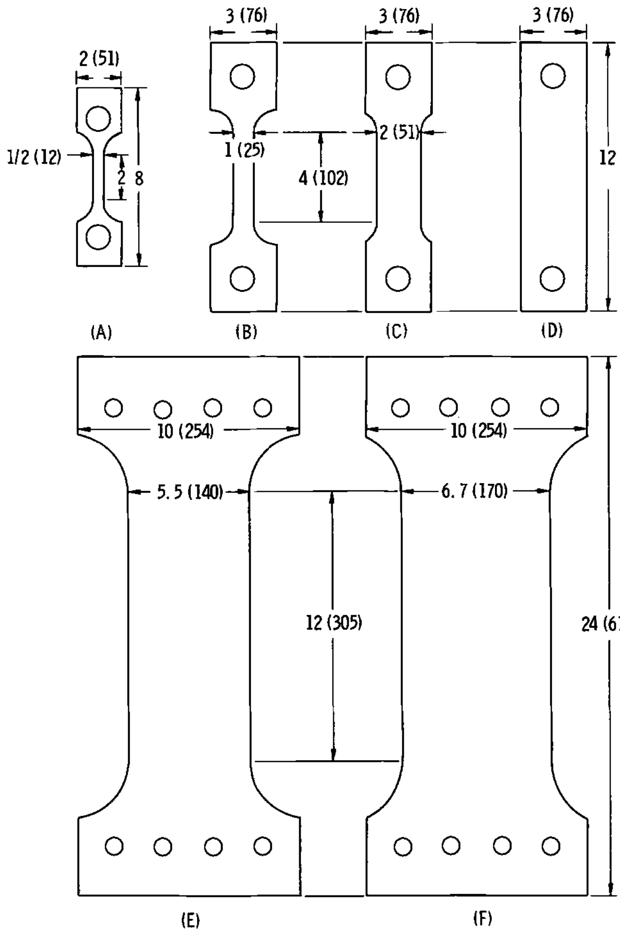

FIG. 5—*Smooth tension and fracture specimens (dimensions in inches or mm).*

107, and 535 kN). For smooth tension tests, differential transformer extensometers were used to measure average strain over a 2-in. (5-cm) gage length. Cryogenic test temperatures were established by immersing the specimen in liquid nitrogen or liquid hydrogen. A vacuum jacketed cryostat with multilayer insulation was used to minimize boiloff. Cryogenic liquid level was maintained several inches above the upper specimen grip, and carbon resistors were used as level sensors.

Results

Nominal fracture toughness values for through crack specimens were calculated with the finite width correction factor proposed by Feddersen

TABLE 3—*Through crack fracture test data.*

Alloy	Test Temperature		Specimen Width, W		Specimen Thickness, t		Initial Crack Length, $2c$		Gross Fracture Stress, σ		Nominal Fracture Toughness, K_{cn}	
	deg F	deg K	in.	mm	in.	mm	in.	mm	ksi	MN/m^2	ksi$\sqrt{\text{in.}}$	MNm$^{-3/2}$
Ti-5Al-2.5Sn	−423	20	2.00	51	0.0624	1.58	0.080	2.0	147.1	1010	58.7	64.5
			1.00	25	0.0616	1.56	0.085	2.2	131.1	904	52.8	58.0
			2.00	51	0.0632	1.61	0.141	3.6	123.0	848	62.9	69.1
			1.00	25	0.0639	1.62	0.172	4.4	115.5	796	66.2	72.7
			2.00	51	0.0632	1.61	0.179	4.5	115.1	794	65.8	72.3
			1.00	25	0.0629	1.60	0.414	10.5	63.9	441	60.1	66.0
			2.00	51	0.0640	1.63	0.420	10.7	78.3	540	67.8	74.5
			1.00	25	0.0640	1.63	0.481	12.2	54.6	376	57.7	63.4
			2.00	51	0.0628	1.60	0.793	20.1	46.8	323	59.1	64.9
			3.00	76	0.0640	1.63	0.988	25.1	48.5	334	66.0	72.5
			3.00	76	0.0639	1.62	0.995	25.3	44.9	310	61.2	67.2
Ti-5Al-2.5Sn	−423	20	1.00	25	0.1115	2.83	0.123	3.1	161.3	1110	86.7	95.3
			2.00	51	0.1122	2.85	0.129	3.3	158.3	1090	84.6	93.0
			1.00	25	0.1126	2.86	0.240	6.1	116.9	806	83.1	91.3
			2.00	51	0.1135	2.88	0.269	6.8	119.0	821	86.0	94.5
			1.00	25	0.1128	2.87	0.360	9.1	90.3	623	80.4	88.3
			2.00	51	0.1128	2.87	0.381	9.7	97.3	671	82.3	90.4
			3.00	76	0.1162	2.95	0.994	25.2	58.3	402	80.5	88.5
			3.00	76	0.1157	2.94	1.051	26.7	55.2	381	79.1	86.9
2014-T6 aluminum	−423	20	3.00	76	0.0613	1.56	0.277	7.0	59.3	409	46.5	51.1
					0.0622	1.58	0.278	7.1	58.8	405	46.0	50.5
					0.0617	1.57	0.557	14.1	46.5	321	49.6	54.5

					0.0600	1.52	0.775	19.7	41.9	289	53.3	58.6
					0.0613	1.56	0.846	21.5	39.5	272	52.6	57.8
					0.0611	1.55	1.032	26.2	34.2	236	50.9	55.9
					0.0604	1.53	1.187	30.1	32.2	222	53.0	58.2
					0.0602	1.53	1.204	30.6	31.5	217	52.2	57.4
					0.0608	1.54	1.399	35.5	28.4	196	53.0	58.2
					0.0611	1.55	1.432	36.4	27.5	190	52.2	57.4
2219-T87 aluminum....	+70	300	5.5	140	0.0676	1.72	0.334	8.5	52.5	362	53.1	58.3
					0.0672	1.71	0.402	10.2	51.3	354	56.1	61.6
					0.0673	1.71	0.515	13.1	49.8	343	60.8	66.8
					0.0676	1.72	0.623	15.8	47.9	330	63.2	69.4
			6.7	170	0.0670	1.70	0.909	23.1	47.3	326	76.0	83.5
					0.0680	1.73	1.004	25.5	46.1	318	77.1	84.7
					0.0682	1.73	1.186	30.1	43.4	299	77.5	85.2
	−320	77	5.5	140	0.0685	1.74	0.332	8.4	63.2	436	64.9	71.3
					0.0687	1.74	0.420	10.7	61.5	424	69.6	76.5
					0.0680	1.73	0.480	12.2	60.2	415	72.1	79.2
					0.0676	1.72	0.621	15.8	57.1	394	75.5	83.0
			6.7	170	0.0673	1.71	0.884	22.5	55.9	385	88.1	96.8
			6.7	170	0.0683	1.73	0.998	25.3	54.6	376	90.9	99.9
			6.7	170	0.0686	1.74	1.203	30.6	51.1	352	91.7	100.8
	−423	20	5.5	140	0.0682	1.73	0.297	7.5	66.7	460	61.3	67.4
					0.0680	1.73	0.400	10.2	64.6	445	67.7	74.4
					0.0672	1.71	0.492	12.5	62.6	432	71.5	78.6
					0.0675	1.71	0.610	15.5	61.5	424	78.2	85.9
			6.7	170	0.0683	1.73	0.825	21.0	58.2	401	83.9	92.2
					0.0676	1.72	0.891	22.6	57.5	396	85.9	94.4
					0.0686	1.74	1.027	26.1	55.7	384	88.9	97.7
					0.0684	1.74	1.184	30.1	53.6	370	91.4	100.4

TABLE 4—*Surface crack fracture test data.*

Alloy	Test Temperature		Specimen Width, W		Specimen Thickness, t		Crack Depth, a		Crack Length, $2c$		Gross Fracture Stress, σ		Apparent Fracture Toughness, K_Q	
	deg F	deg K	in.	mm	in.	mm	in.	mm	in.	mm	ksi	MN/m²	ksi$\sqrt{\text{in.}}$	MN/m$^{3/2}$
Ti-5Al-2.5Sn, 0.06-in. (1.6-mm)	−423	20	1.00	25	0.0630	1.60	0.022	0.56	0.089	2.26	207.6	1430	51.8	56.9
			1.00	25	0.0628	1.60	0.024	0.61	0.078	1.98	207.5	1430	49.8	54.7
			1.00	25	0.0631	1.60	0.027	0.69	0.065	1.65	213.3	1470	47.1	51.8
			2.00	51	0.0635	1.61	0.027	0.69	0.075	1.91	182.7	1260	42.8	47.0
			1.00	25	0.0636	1.62	0.031	0.79	0.077	1.96	180.8	1250	43.1	47.4
			2.00	51	0.0643	1.63	0.033	0.84	0.099	2.51	169.0	1170	45.4	49.9
			2.00	51	0.0621	1.58	0.034	0.86	0.132	3.35	152.3	1050	46.0	50.5
			1.00	25	0.0648	1.65	0.037	0.94	0.102	2.59	153.5	1060	42.0	46.1
			2.00	51	0.0635	1.61	0.038	0.97	0.122	3.10	152.0	1050	45.3	49.8
			1.00	25	0.0647	1.64	0.040	1.02	0.123	3.12	137.9	951	41.3	45.4
			2.00	51	0.0641	1.63	0.040	1.02	0.128	3.25	145.7	1000	44.6	49.0
			1.00	25	0.0650	1.65	0.041	1.04	0.147	3.73	130.0	896	42.1	46.3
			2.00	51	0.0628	1.60	0.046	1.17	0.158	4.01	107.4	741	37.1	40.8
			1.00	25	0.0640	1.63	0.050	1.27	0.173	4.39	102.4	706	37.9	41.6
			2.00	51	0.0646	1.64	0.051	1.30	0.175	4.45	98.0	676	36.6	40.2
			2.00	51	0.0646	1.64	0.056	1.42	0.190	4.83	96.7	667	40.2	44.2
			1.00	25	0.0642	1.63	0.056	1.42	0.200	5.08	101.5	700	43.8	48.1
			2.00	51	0.0631	1.60	0.031	0.79	0.297	7.54	138.3	954	48.2	53.0
			1.00	25	0.0630	1.60	0.033	0.84	0.286	7.26	136.9	944	48.8	53.6
			1.00	25	0.0639	1.62	0.033	0.84	0.300	7.62	136.9	944	49.0	53.8
			1.00	25	0.0640	1.63	0.034	0.86	0.391	9.93	143.6	990	54.2	59.6

			2.00	51	0.0637	1.62	0.035	0.89	0.399	10.13	138.0	952	52.9	58.1
			1.00	25	0.0622	1.58	0.037	0.94	0.393	9.98	120.4	830	47.3	52.0
			2.00	51	0.0639	1.62	0.043	1.09	0.590	14.99	111.7	770	50.0	54.9
			2.00	51	0.0633	1.61	0.045	1.14	0.351	8.92	106.1	732	45.6	50.1
			2.00	51	0.0638	1.62	0.048	1.22	0.782	19.86	85.1	587	42.4	46.6
			2.00	51	0.0627	1.59	0.049	1.24	0.820	20.83	80.6	556	41.5	45.6
Ti-5Al-2.5Sn, 0.11-in. (2.9-mm).......	−423	20	1.00	25	0.1157	2.94	0.023	0.58	0.118	3.00	207.6	1430	56.9	62.5
			2.00	51	0.1122	2.85	0.037	0.94	0.129	3.28	195.5	1350	59.8	65.7
			1.00	25	0.1133	2.88	0.043	1.09	0.153	3.89	184.9	1270	61.3	67.4
			1.00	25	0.1129	2.87	0.056	1.42	0.179	4.55	162.1	1120	58.4	64.2
			1.00	25	0.1128	2.87	0.068	1.73	0.227	5.77	144.0	993	58.6	64.4
			2.00	51	0.1147	2.91	0.073	1.85	0.247	6.27	139.9	965	59.6	65.5
			1.00	25	0.1111	2.82	0.077	1.96	0.290	7.37	118.9	820	54.8	60.2
			2.00	51	0.1143	2.90	0.084	2.13	0.291	7.39	129.0	889	61.2	67.2
			1.00	25	0.1161	2.95	0.097	2.46	0.342	8.69	105.4	727	57.1	62.7
			2.00	51	0.1119	2.84	0.101	2.57	0.337	8.56	110.4	761	65.3	71.8
2014-T6 aluminum......	−423	20	3.00	76	0.0622	1.58	0.034	0.86	0.206	5.23	72.1	497	25.7	28.2
			2.99	76	0.0620	1.57	0.035	0.89	0.213	5.41	70.8	488	25.6	28.1
			2.99	76	0.0615	1.56	0.038	0.97	0.311	7.90	63.4	437	25.4	27.9
			2.99	76	0.0615	1.56	0.042	1.07	0.403	10.24	55.1	380	24.1	26.5
			3.01	76	0.0600	1.52	0.044	1.12	0.232	5.89	66.2	456	27.4	30.1
			3.00	76	0.0613	1.56	0.044	1.12	0.265	6.73	63.1	435	26.8	29.4
			2.99	76	0.0605	1.54	0.046	1.17	0.457	11.61	51.7	356	24.7	27.1
			2.99	76	0.0612	1.55	0.051	1.30	0.609	15.47	47.8	330	26.6	29.2
			3.00	76	0.0603	1.53	0.054	1.37	1.275	32.39	31.4	217	21.5	23.6
			3.01	76	0.0600	1.52	0.055	1.40	1.115	28.32	33.6	232	24.9	27.4
			3.00	76	0.0603	1.53	0.055	1.40	1.363	34.62	29.6	204	21.7	23.8
			3.00	76	0.0619	1.57	0.058	1.47	0.198	5.03	66.7	460	34.2	37.6

([1], pp. 77–79). With this correction Eq 1 becomes

$$K_{cn} = \sigma\sqrt{W\theta\sec\theta} \text{ where } \theta = \frac{\pi}{2}\left(\frac{2c}{W}\right) + \frac{1}{2W}\left(\frac{K_{cn}}{\sigma_{ys}}\right)^2 \quad (4)$$

Apparent fracture toughness (K_Q) values for surface crack specimens were calculated from Eq 1*b* (rearranged) and the free surface correction factor of Ref *11*. Fracture test results and some calculated quantities are listed in Tables 3 and 4.

Titanium Alloy

Figure 6 presents fracture stresses for through cracks and surface cracks in the thinner (0.06-in.) titanium sheet at −423 F (20 K). The surface crack tests are grouped according to depth to thickness ratio. The experimental trends are generally in good agreement with the predicted trends of Fig. 3. Nominal fracture toughness (K_{cn}) for the through crack specimens was essentially constant (62 ksi$\sqrt{\text{in.}}$ (68 MN/m$^{3/2}$) avg). Apparent fracture toughness K_Q for the surface crack tests was reasonably constant (47 ksi$\sqrt{\text{in.}}$ (52 MN/m$^{3/2}$) avg) for all but the seven specimens with cracks deeper than 70 percent of the thickness. Note (Fig. 6) that for the five of these with short cracks (2c ~ 0.18 in.) fracture stresses are within the scatterband for through crack tests. Using the average K_Q value (47 ksi$\sqrt{\text{in.}}$), Irwin's plastic zone size is between 14 and 29 percent of the uncracked ligament depth for the seven deviant tests. However, as discussed

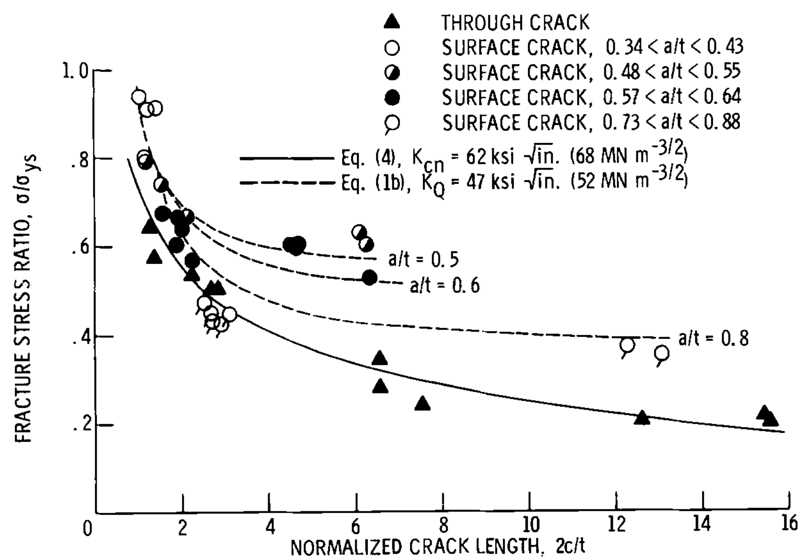

FIG. 6—*Fracture stress for Ti-5Al-2.5Sn ELI specimens 0.06 in. (1.6 mm) thick (−423 F (20 K); yield strength, 228.0 ksi (1570 MN/m²)).*

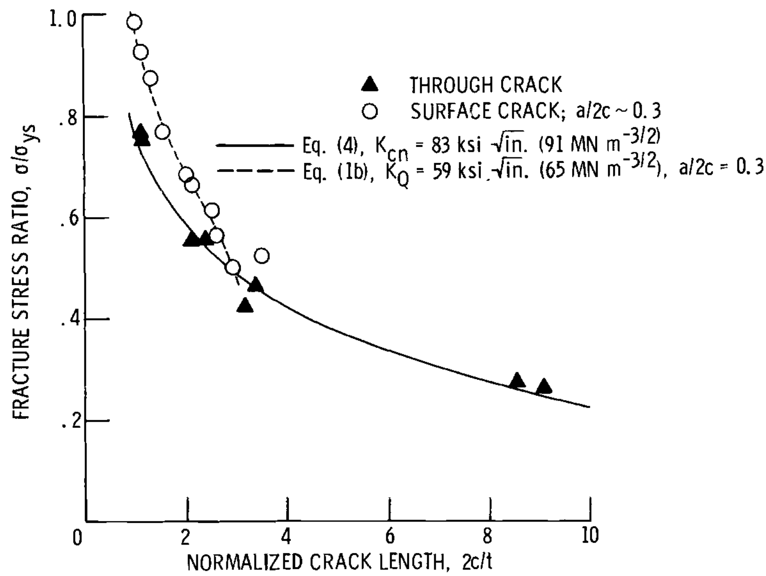

FIG. 7—*Fracture stress for Ti-5Al-2.5Sn ELI specimens 0.11 in. (2.9 mm) thick (−423 F (20 K); yield strength, 211 ksi (1450 MN/m²)).*

earlier, this expression is probably a conservative (low) estimate of the actual plastic zone size, which may be several times larger.

Figure 7 presents fracture stresses for through cracks and surface cracks in the thicker (0.11-in.) titanium sheet, also at −423 F (20 K). Here the surface crack shapes remained essentially constant ($a/2c = 0.3$ approximately) as crack depth was varied. Nominal fracture toughness (K_{cn}) for through crack specimens was essentially constant (83 ksi$\sqrt{\text{in.}}$ (91 MN/$m^{3/2}$) avg), as was apparent toughness K_Q for surface crack specimens (59 ksi$\sqrt{\text{in.}}$ (65 MN/$m^{3/2}$) avg). Note that fracture stresses for the three deepest surface crack tests lie within or near the scatterband for through crack tests. For these three specimens, Irwin's plastic zone size (K_Q = 59 ksi$\sqrt{\text{in.}}$) is between 13 and 40 percent of the uncracked ligament depth.

Even though both thicknesses are from the same heat, the K_Q and K_{cn} average values are about 13 percent higher (and strengths lower) for the thicker gage. However, the K_Q average values for both are within the range of K_{Ic} values reported in Ref *16* for much thicker specimens.

Aluminum Alloys

Figure 8 presents fracture stresses for through cracks and surface cracks in 2014-T6 aluminum sheet (0.06 in. (1.6 mm) thick) at −423 F (20 K). Note that only for the shortest cracks is there any apparent difference between fracture stresses for through cracks and for surface cracks. Nominal fracture toughness (K_{cn}) was approximately constant (52 ksi$\sqrt{\text{in.}}$ (57 MN/m$^{3/2}$) avg) for all but the two shortest through cracks. Apparent toughness K_Q was also constant (26 ksi$\sqrt{\text{in.}}$ (28 MN/m$^{3/2}$) avg) for all but the four deepest surface cracks.

For these four, Irwin's plastic zone size (based on 26 ksi$\sqrt{\text{in.}}$) was deeper than any uncracked ligament. For the eight other specimens, Irwin's plastic zone size was between 26 and 72 percent of the depth of the uncracked ligaments. However, even though constant, the K_Q values are unusually low. The surface crack K_Q values reported in Ref *17* for 2014-T62 alloy 0.5 in. (13 mm) thick are nearly twice as large. If based on the Ref *17* values, Irwin's plastic zone would be deeper than any uncracked ligament. Analysis according to Ref *11*, where plastic zone size is related to fracture stress rather than stress intensity, also indicates that the plastic zone did extend completely through the thickness prior to fracture for every test.

Figure 9 presents fracture stresses for through cracks and surface cracks in 2219-T87 aluminum sheet (0.07 in. (1.7 mm) thick) at ambient temperature, −320, and −423 F (300, 77, and 20 K). The surface crack data are taken from Ref *15*; through crack specimens from the same lot of material

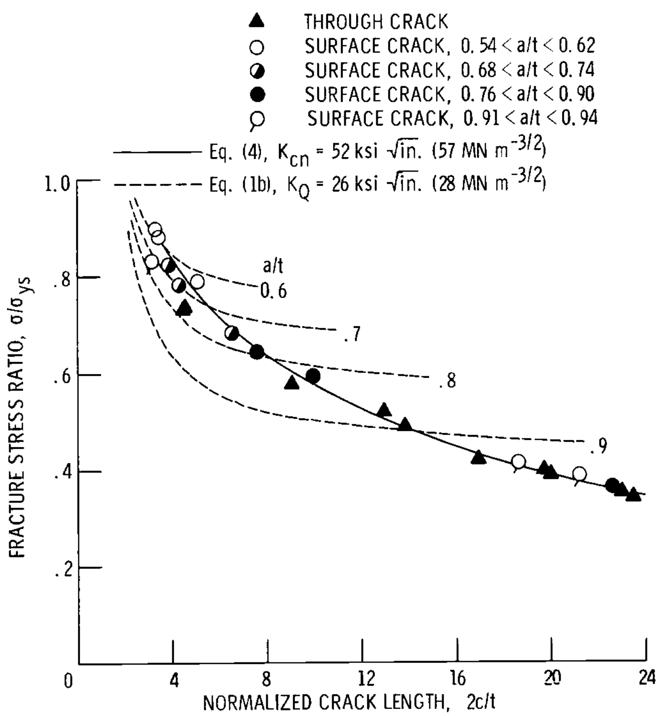

FIG. 8—*Fracture stress for 2014-T6 aluminum specimens 0.06 in. (1.6 mm) thick (−423 F (20 K); yield strength, 80.3 ksi (554 MN/m²)).*

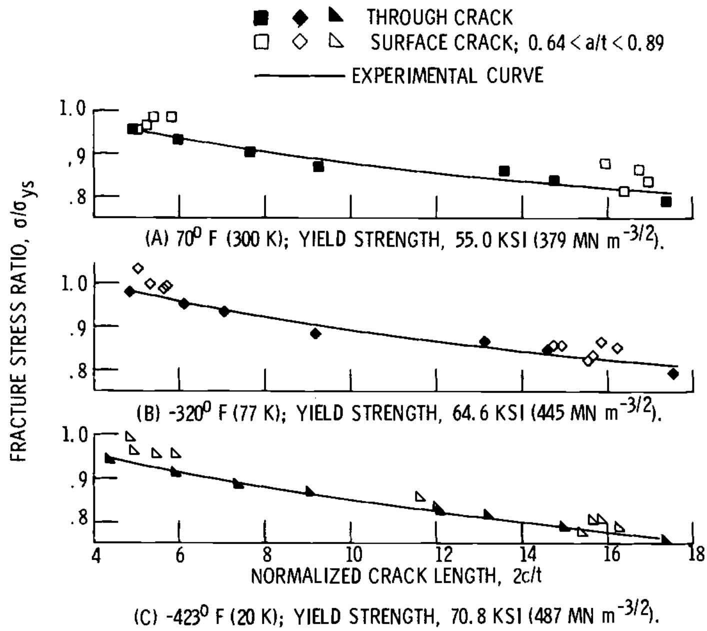

FIG. 9—*Fracture stress 2219-T87 aluminum specimens 0.07 in.* (*1.7 mm*) *thick; surface crack data from Ref* 15.

were tested at the Lewis Research Center. Neither nominal toughness (K_{cn}) nor apparent toughness K_Q were constant at any temperature, and the curves of Fig. 9 were merely drawn through the through crack data. Note that again there is little difference in fracture stresses for surface cracks and for through cracks of the same length. Based on the estimated K_{Ic} values of Ref *15*—47 ksi$\sqrt{\text{in.}}$ at 70, 50 ksi$\sqrt{\text{in.}}$ at −320 and −423 F (52 MN/m$^{3/2}$ at 300, 55 MN/m$^{3/2}$ at 77 and 20 K)—the Irwin plastic zone sizes were greater than all uncracked ligament depths. Thus it is fairly certain that the surface crack plastic zones penetrated the thickness prior to fracture in every test.

Discussion of Results

The constant K_{cn} concept is not sufficient to characterize through crack fracture in the relatively tough 2219-T87 alloy. But for the less tough titanium and 2014-T6 aluminum alloys, it relates fracture stress to original crack length adequately over the range of these tests.

The characterization of surface crack fracture is not as straightforward. However, the results are consistent if they are classified according to the relative depths of the plastic zone and the uncracked ligament. For most of the titanium specimens, where Irwin's plastic zone size was less than about 13 percent of the uncracked ligament depth, K_Q values were essentially constant and the plane strain model (Eq 1*b*) seems appropriate. For all the aluminum specimens, the plastic zone is believed to have extended completely through the thickness. Here fracture appears to be strongly related to crack length and the mixed mode fracture toughness (K_{cn}). The behavior of the remainder of the titanium specimens is harder to classify, but this may be due to the approximate nature of the plastic zone size term.

As discussed earlier, Irwin's surface crack analysis should be usable if the actual plastic zone size is small with respect to the depth of the uncracked ligament. These tests suggest an approximate limit. If Irwin's plastic zone term is less than about one tenth of the depth of the uncracked ligament, the plane strain model appears to be applicable even for thin sections. However, the parameter K_Q (which may or may not be equal to the plane strain toughness K_{Ic}) must be carefully determined. When the plastic zone is greater than the depth of the uncracked ligament, final fracture usually appears to be related to crack length and mixed mode fracture toughness.

The analysis and the preceeding discussion assume that surface cracks do not propagate until rapid fracture occurs. However, some investigators have recently observed stable subcritical growth of surface cracks in some materials. Just prior to fracture, such a crack could be larger than its original dimensions but not yet through the thickness. In such a case, a K_Q value based on original crack depth and maximum load would be erroneously low. Subcritical growth might account for some (but not all) of the observed deviations of K_Q from a constant value.

Concluding Remarks

The experiments reported here indicate that the fracture behavior of thin sections containing surface cracks may be strongly influenced by the ratio of the crack tip plastic zone size to the ligament depth (thickness minus crack depth). The experimental results can be summarized as follows:

1. When the Irwin plastic zone size at fracture was less than about one tenth of the ligament depth, fracture behavior was, in general, as predicted by plane strain theory.

2. When the plastic zone size was greater than the ligament depth, fracture stresses for surface crack specimens were nearly the same as for specimens with through cracks of the same original length. It should be recognized that these conclusions may not be applicable to other materials or thicknesses or both, and more definitive tests are required to either confirm or correct them.

Based on analysis using current fracture mechanics theory, as supported but limited by these tests, it can be postulated that

1. Current fracture mechanics methods can be applied to leak-before-

burst problems of thin-walled pressure vessels, but only if the plastic zone at failure is small with respect to the uncracked ligament. If so, leaks can be expected only for narrow ranges of crack geometry and material properties.

2. If the plastic zone is expected to penetrate the thickness prior to failure, current analytical methods cannot predict whether a vessel will leak or burst at fracture. Under these circumstances, a cracked tension specimen may not adequately simulate a cracked pressure vessel.

References

[1] Brown, W. F., Jr., and Srawley, J. E., *Plane Strain Crack Toughness Testing of High Strength Metallic Materials, ASTM STP 410*, American Society for Testing and Materials, 1967.

[2] Irwin, G. R., *Journal of Applied Mechanics*, JAMCA, Vol. 29, No. 4, Dec. 1962, pp. 651–654.

[3] Proposed Method of Test for Plane Strain Fracture Toughness of Metallic Materials, *Annual Book of ASTM Standards*, Part 31, May 1969, pp. 1099–1114.

[4] Amateau, M. F. and Steigerwald, E. A., "Test Methods for Determining Fracture Toughness of Metallic Materials," Technical Report AFML-TR-67-145, Air Force Materials Laboratory, Dayton, Ohio, Sept. 1967.

[5] Srawley, J. E. and Brown, W. F., Jr., in *Symposium on Fracture Toughness Testing and its Applications, ASTM STP 381*, American Society for Testing and Materials, 1965, pp. 133–198; also available as NASA TN D-2599, 1965.

[6] Orange, T. W., "Fracture Toughness of Wide 2014-T6 Aluminum Sheet at −320 F," NASA Report TN D-4017, National Aeronautics and Space Administration, Cleveland, Ohio, 1967.

[7] Kuhn, P., *Materials Research and Standards*, MTRSA, Vol. 8, No. 9, Sept. 1968, pp. 21–26.

[8] Rice, J. R. in *Symposium on Fatigue Crack Propagation, ASTM STP 415*, American Society for Testing and Materials, 1967, pp. 247–311.

[9] Hahn, G. T. and Rosenfield, A. R., "Plastic Flow in the Locale on Notches and Cracks in Fe-3Si Steel Under Conditions Approaching Plane Strain," Report SSC-191, Ship Structure Committee, Department of the Navy, Nov. 1968.

[10] Ayres, D. J., "A Numerical Procedure for Calculating Stress and Deformation Near a Slit in a Three-Dimensional Elastic-Plastic Solid," NASA Report TN D-4717, National Aeronautics and Space Administration, 1968.

[11] Kobayashi, A. S. and Moss, W. L. in *Fracture; Proceedings of the Second International Conference on Fracture*, Chapman and Hall Ltd., 1969, pp. 31–45.

[12] Irwin, G. R. and Srawley, J. E., *Materialprüfung*, MTPRA, Vol. 4, No. 1, Jan. 20, 1962, pp. 1–11.

[13] Anderson, R. B. and Sullivan, T. L., "Fracture Mechanics of Through-Cracked Cylindrical Pressure Vessels," NASA Report TN D-3252, National Aeronautics and Space Administration, 1966.

[14] Eiber, R. J., Maxey, W. A., Duffy, A. R., and McClure, G. M., "Behavior of Through-Wall and Surface Flaws in Cylindrical Vessels," presented at the National Symposium on Fracture Mechanics, Lehigh University, Bethlehem, Pa., June 1968 (to be published in *Journal of Engineering Fracture Mechanics*).

[15] Masters, J. N., Haese, W. P., and Finger, R. W., "Investigation of Deep Flaws in Thin Walled Tanks," NASA Report CR-72606, Boeing Company, Dec. 1969.

[16] Pyle, R., Schillinger, D. E., and Carman, C. M., "Plane Strain Fracture Toughness and Mechanical Properties of 2219-T87 Aluminum and 5Al-2.5Sn ELI Titanium Alloy Weldments and One Inch Thick 5Al-2.5Sn ELI Titanium Alloy Plate," Report FA-R-1897, NASA Report CR-72154, Frankford Arsenal, Sept. 1968.

[17] Hall, L. R., "Plane-Strain Cyclic Flaw Growth in 2014-T62 Aluminum and 6Al-4V (ELI) Titanium," Report DR-114465-1, NASA Report CR-72396, Boeing Co., Nov. 1968.